XII. PLASMA MAGNETOHYDRODYNAMICS AND ENERGY CONVERSION[*]

Prof. G. A. Brown	Dr. E. S. Pierson	B. T. Lubin
Prof. R. S. Cooper	M. T. Badrawi	C. A. McNary
Prof. W. H. Heiser	J. L. Coggins	R. P. Porter
Prof. M. A. Hoffman	R. K. Edwards	S. Sacks
Prof. W. D. Jackson	J. R. Ellis, Jr.	C. V. Smith, Jr.
Prof. J. L. Kerrebrock	J. W. Gadzuk	A. Solbes
Prof. J. E. McCune	T. K. Gustafson	R. J. Thome
Prof. A. H. Shapiro	R. W. King	B. D. Wessler
Prof. R. E. Stickney	G. B. Kliman	J. C. Wissmiller
Dr. J. B. Heywood	A. G. F. Kniazzeh	G. W. Zeiders

A. EXPERIMENTS WITH A LIQUID-METAL MAGNETOHYDRODYNAMIC WAVEGUIDE

There have been several attempts in the last few years to show the existence of Alfvén waves in a liquid-metal waveguide. Gothard[1,2] designed an experimental waveguide and, using it as a resonator, obtained preliminary data. His equipment was used by Jackson and Carson[3] to obtain more conclusive and extensive data. These investigators were able to obtain field-dependent resonances in the waveguide at frequencies corresponding to those of TM Alfvén wave modes. They were not able, however, to see anything conclusive with a coil probe which was located in the waveguide cavity.

In this investigation, the objective was to display the waves in the most direct manner so that it could be used in a film, entitled "Magnetohydrodynamics," which is now being made for the Fluid Mechanics Film Series produced by Educational Services Incorporated. To reduce attenuation, the walls of the Gothard waveguide were lined with copper and the ends were insulated to obtain boundary conditions that correspond closely to the theoretical model used by Reid.[4] The excitation system was also changed from a disk exciter, which produces TM modes, to a copper cylindrical center conductor, which produces TEM modes. Thus the waveguide was essentially a coaxial line filled with a liquid metal. Sodium-potassium alloy (NaK) was again used as the working fluid. The excitation current was changed to a square wave so that the progress of the wave front past two stationary probe coils could be observed.

The complete waveguide assembly is shown in Figs. XII-1 through XII-4; it can be seen that the waveguide is a copper can fitting into the original stainless-steel structure developed by Gothard. The center post is made of solid copper with an outside diameter of 2.5 cm, and the length of the waveguide is 15 cm. This is 3 cm smaller than the total length of the magnet gap, and allows clearance for the input cables to be attached to the
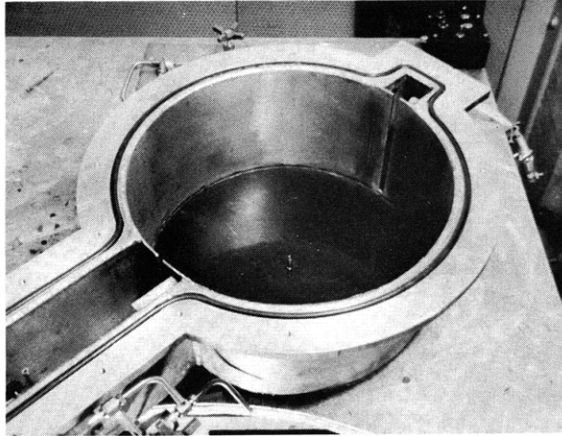

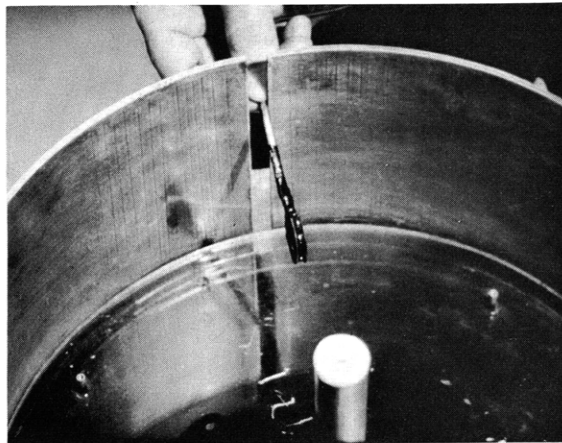Fig. XII-1. Gothard waveguide showing insulated lower end.

Fig. XII-2. Copper insert with center post.

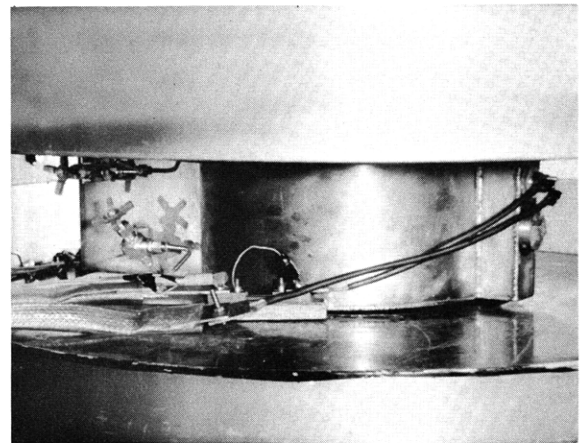Fig. XII-3. Search coil position in the waveguide cavity.

Fig. XII-4. Waveguide positioned in magnetic field.

center of the guide to obtain current distribution independently of the ϕ-coordinate. The field probe consisted of a solenoid, 3/8 inch in diameter, with 600 turns of No. 37 wire laid in epoxy. The output of the coils was isolated from the rest of the system by transformers to eliminate the effects of ground currents from the measuring circuits. The transformer output was then amplified approximately 40 db, and the final output was displayed on a Tektronix oscilloscope.

The applied magnetic field was 0.8 weber/meter^2, and the exciting current was a 10-cps square wave with an amplitude of 100 amps. The fluid properties of the NaK alloy used in the experiment were: density $\rho = 0.85 \times 10^3$ kg/m^3; electrical conductivity $\sigma = 2.4 \times 10^6$ mhos/meter. The Alfvén wave velocity v_a is given by $v_a = B_0/\sqrt{\mu_0 \rho}$, which, under the experimental conditions used, was calculated to be $v_a = 24.5$ meters/second. Thus the wave should transverse the length of the waveguide in

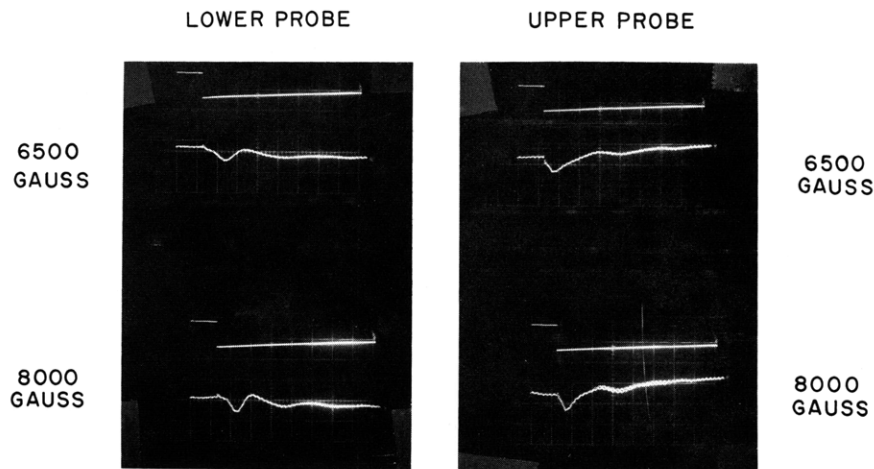LOWER PROBE   UPPER PROBE

Fig. XII-5.   Drive current and probe waveforms.   Upper
             trace: exciting current.   Lower trace: probe
             voltage waveform.   (Time scale, 5 msec/cm.)

6.2 msec. Reproductions of the typical oscilloscope traces, obtained by using a Polaroid camera, are shown in Fig. XII-5. Reflections are clearly visible and serve to confirm the fact that the observed phenomenon has the character of wave motion. The arrival times of the initial wavefront at the first (upper) and second (lower) probes were 2.34 msec and 4.90 msec, respectively. The measured velocity was estimated to be 23.0 m/sec, and the upper and lower probes were calculated to be 5.7 cm and 11.9 cm, respectively, from the top of the waveguide. Good agreement was obtained with the predicted behavior of a TEM Alfvén mode in a cylindrical waveguide, and an error of ~6 per cent arises largely from the difficulty of locating the exact arrival time in the presence of a substantial amount of wave dispersion.

W. D. Jackson, B. D. Wessler, G. B. Kliman

References

1. N. Gothard, S. M. Thesis, Department of Electrical Engineering, M. I. T., 1962.

2. N. Gothard, Excitation of hydromagnetic waves in a highly conducting liquid, Phys. Fluids 7, 1784 (1964).

3. W. D. Jackson and J. F. Carson, Quarterly Progress Report No. 72, Research Laboratory of Electronics, M. I. T., January 15, 1964, p. 149.

4. M. H. Reid, S. B. Thesis, Department of Electrical Engineering, M. I. T., 1962.

B. HALL PARAMETER – CONDUCTIVITY INSTABILITIES IN MAGNETOGASDYNAMIC FLOW

McCune[1] has analyzed instabilities in a slightly ionized plasma, which are due to fluctuations in the local conductivity and Hall parameter. Essentially, his work expanded the analysis of Hall parameter instabilities previously conducted by Velikhov.[2] McCune's analysis differed from Velikhov's with respect to both model and approach: McCune used a dispersion relation approach, while Velikhov used an energy approach. It appears that stability criteria are most readily obtained for McCune's model by using Velikhov's approach.

Consider a plasma with a low magnetic Reynolds number, slight ionization (less than 0.1 per cent), in the presence of a strong magnetic field so that the Hall parameter is greater than unity. The pertinent linearized first-order electromagnetic, fluid-mechanic, and constitutent equations are listed below. All terms, except physical constants that have zero subscripts, indicate zero-order terms. The wave disturbance is in a plane perpendicular to the magnetic field, parallel or antiparallel to the current, one-dimensional, and proportional to $\exp[i(\omega t - \overline{k} \cdot \overline{r})]$.

1. $\dfrac{\partial \rho}{\partial t} + \rho_o \nabla \cdot \overline{v} = 0$ $\qquad$ $\Omega_o = \dfrac{w}{\nu_o}$

2. $\nabla \cdot \overline{j} = 0$ $\qquad$ w = cyclotron frequency

3. $\nabla \times \overline{e} = 0$ $\qquad$ $\nu_o = \dfrac{1}{\tau}$ = collision frequency

4. $\rho_o \dfrac{\partial v}{\partial t} + \nabla p = \overline{j} \times \overline{B}_o$ $\qquad$ Ω_o = Hall parameter

5. $\overline{j} + \overline{j} \times \overline{\Omega}_o + \overline{J}_o \times \overline{\Omega} = \sigma_o(\overline{e} + \overline{v} \times \overline{B}_o) + \sigma\overline{E}_o$

If we combine the x component of the last equation with the remaining four equations we find that

$$j_x = -J_o \Omega_o \left(\frac{\Omega}{\Omega_o}\right) + \sigma_o E_{ox} \left(\frac{\sigma}{\sigma_o}\right) + \sigma_o B_o v.$$

The perturbation current is composed of three parts: perturbation currents caused by (a) local fluctuations in the Hall parameter, (b) fluctuations in the conductivity, and (c) the electromotive force. This total perturbation current, together with the uniform magnetic field, will produce a force that will cause instability if the force and velocity are in the same direction. For a slightly ionized gas the conductivity will increase as the temperature to the power a (where a is ~13). Also,

$$\nu_o = \left(\frac{8kT_o}{\pi M_e}\right)^{1/2} N_o Q_N,$$

where Q_N is the collision cross section between electrons and neutrals, and N_o is the neutral density. Therefore,

$$\frac{\sigma}{\sigma_o} = a \frac{T}{T_o}$$

and

$$\frac{\Omega}{\Omega_o} = -\frac{1}{2} \frac{T}{T_o} - \frac{N}{N_o}.$$

It can be shown that for small temperature variations the conductivity also depends upon density variations so that

$$\frac{\sigma}{\sigma_o} = a \frac{T}{T_o} - \frac{1}{2} \frac{\rho}{\rho_o}.$$

The density dependence can be neglected whenever $a \approx 13$ and $\gamma = \dfrac{C_p}{C_v}$ is greater than approximately 1.2.

If we use this relationship and assume the equation of state for an ideal gas, we find that

$$-j_x B_o \left\{ 1 + i\frac{1}{2} \frac{J_o B_o \Omega_o}{p_o k} + i \frac{a E_{ox} B_o \sigma_o}{p_o k} \right\} = -\frac{J_o B_o \Omega_o}{2} \left[\gamma \left(\frac{v_{ph}}{a_o}\right)^2 + 1 \right] \frac{k}{\omega} v - \sigma_o B_o^2 v$$

$$-a E_{ox} B_o \sigma_o \left[\gamma \left(\frac{v_{ph}}{a_o}\right)^2 - 1 \right] \frac{k}{\omega} v.$$

If we consider short wavelengths such as

$$\frac{a J_o B_o \Omega_o}{p_o k} \ll 1,$$

or equivalently

$$\lambda \ll \frac{2\pi p_o}{J_o B_o \Omega_o} = L_i,$$

where L_i is an interaction length, the resulting energy equation is

$$j_x v^* B_o = |v|^2 \left\{ -\sigma_o B_o^2 - \frac{J_o B_o \Omega_o}{2} \left[\gamma \left(\frac{v_{ph}}{a_o} \right)^2 + 1 \right] \frac{k}{\omega} \right.$$
$$\left. - J_o B_o \Omega_o a \left[\gamma \left(\frac{v_{ph}}{a_o} \right)^2 - 1 \right] \frac{k}{\omega} \right\}.$$

The terms on the right-hand side are due to the electromotive force, Hall parameter fluctuation, and conductivity fluctuation perturbation currents, respectively. For short wavelengths such that

$$\lambda \ll 2\pi \frac{(p_o C_o T_o) v_{ph}}{\left(J_o^2 / \sigma_o \right) \Omega_o}$$

the phase velocity is approximately equal to the speed of sound. For $\gamma = 1$ and for stability the current density must satisfy

$$J_o < \frac{\sigma_o v_{ph} B_o}{\Omega_o} = J_{CR}.$$

This is Velikhov's criterion; it is recovered here because we have assumed that the conductivity is a function only of temperature.

If we assume that $\frac{1}{2}(\gamma+1)$ is almost one order of magnitude less than $a(\gamma-1)$, for stability, we have

$$J_o < \frac{J_{cr}}{a(\gamma-1)}.$$

In this case the conductivity fluctuation instability dominates. In fact, we see that this will be the case whenever

$$\gamma > \frac{2\alpha + 1}{2\alpha - 1}.$$

Recently, McCune[3] arrived at similar conclusions by analyzing growth rates governed by an appropriate dispersion relation.

We conclude that for practical cases of interest the conductivity fluctuation instability will be present and will dominate whenever a critical current density is exceeded. It should be emphasized that this conductivity instability would not exist without the presence of the Hall effect.

K. R. Edwards

References

1. J. E. McCune, Wave-Growth and Instability in Partially Ionized Gases, Report AMP 136, Avco-Everett Research Laboratory, 1964.

2. E. P. Velikhov, Hall Instability of Current Carrying Slightly Ionized Gases, Symposium on Magnetoplasmadynamic Electric Power Generation, Kings College, University of Durham, Newcastle-upon-Tyne, England, 1962.

3. J. E. McCune, Linear Theory of an MHD Oscillator, Report 198, Avco-Everett Research Laboratory, December 1964.

C. NONLINEAR EFFECTS OF FLUCTUATIONS ON MAGNETOHYDRODYNAMIC PERFORMANCE

Recently, attention[1-4] has been given to the possibility of the appearance of certain types of wave amplification mechanisms ("instabilities") in slightly ionized plasmas, and to the question of their importance in magnetohydrodynamic applications. Among the instabilities investigated thus far, in particular, two stand out as potentially important for MHD machines operating at moderate to high Hall parameters. One of these, the wave instability first noted by Velikhov,[2] and further discussed by the present author,[3] involves coupling between acoustic wave modes and the Hall effect, and can have a sufficiently high growth rate to be significant in contemplated devices.[3,5] This acoustic instability should be observed most strongly (although not exclusively) whenever the electrons are moderately well-coupled energetically to the heavier species of the gas.[3] In contrast, the second kind of instability, first noted by Kerrebrock,[4] is potentially important when the electrons are only weakly coupled to the heavy neutrals in a slightly ionized gas. In the last case, wave motion (involving only the electrons in the limit of very weak coupling) becomes possible through the competition between the electric field and gradient-induced electron diffusion, and amplification of this motion can occur in the presence of a magnetic field.

It has recently been demonstrated[5] that the Velikhov instability is potentially important in large, combustion-driven MHD devices operating with high Hall coefficients,

especially with certain geometries, and at particular acoustic resonant frequencies. Similarly, the Kerrebrock instability is likely to play an especially important role if significant nonequilibrium ionization, for example, is seeded, noble-gas plasmas, is realized. It should be emphasized, however, that the acoustic (Velikhov) instability can also be important in slightly ionized plasmas of this last kind because, even with weak energy coupling between the electrons and heavy species, there is still a direct dependence of the Hall parameter on the gas density.[2,3] This means that acoustic fluctuations — however induced — may have important effects on the DC performance of any MHD device that is intended for use with high Hall parameters.

It should be recognized that experience has shown[6] that the moderate and large-scale combustion-driven MHD generators (of the Faraday type and having linear geometry) that have been run actually operate relatively smoothly. The turbulence level in such devices does not appear to be higher than that expected from normal gasdynamic effects. This is consistent with the author's calculations,[5] which have shown in effect that for linear MHD Faraday-type generators, the generator "system" (plasmas, plus boundaries and external circuitry) is stable at all frequencies to the Velikhov mode, below a certain value of the product $\Omega_o M_o h$, where Ω_o is the DC value of the Hall coefficient, M_o is the DC Mach number, and h is the duct height. (A more precise statement of this condition has been given elsewhere.[5]) Until the present time, MHD generators have either been sufficiently small or have been operated at sufficiently low values of $\Omega_o M_o$ to avoid instability even at the resonant frequencies previously discussed.[5]

This result, however, is strongly dependent on the boundary conditions inherent in Faraday-type generators of duct geometry. Such boundary conditions lead in general to quick reflection and damping of the dominant unstable modes (except at resonance[5]).

Such over-all stability of the "system" cannot be expected with certain Hall generator or accelerator geometries, for which the cathode does not present a simple reflecting surface. Indeed, Klepeis and Rosa[7] have observed strong fluctuations at acoustic frequencies in an MHD disc Hall generator.

We are led to conclude that instabilities of the Velikhov type may be important for any sufficiently large MHD device at particular (resonant) frequencies; and for certain geometries (especially Hall generators) they may appear over a much broader frequency spectrum. Less is known about the Kerrebrock instability, but it seems likely that similar conclusions may be reached.

It is important to investigate the possible effect of fluctuations of this kind upon the DC (time-averaged) behavior of MHD devices. This investigation will also be decisive in establishing the maximum AC power level of MHD generator oscillators of the type already discussed.[5]

1. Recent Results

When an MHD device is subject to AC fluctuations, the steady-state amplitude of the "unstable" modes is determined, in conjunction with the external circuitry, by certain internal nonlinear effects which limit the wave amplitudes. These effects are present, as we shall show, because the DC (time-averaged) fields are affected by nonlinear wave interaction, and the wave amplitudes and other wave characteristics, in turn, are functions of the DC fields. For example, the AC impedance of an MHD oscillator,[5] through such effects, becomes a function of the AC amplitudes, and its AC power output can be determined for any given external AC load.

In a recent paper[8] the present author has presented an approximate theory, analogous to the elementary theory of turbulence in ordinary gasdynamics, as a means of relating the DC electric fields and DC currents to the magntiude of the AC fluctuations. More precisely, it is shown that the main power-carrying DC current and the DC "Hall field" are both reduced by correlations of the AC fluctuations. This results physically because the time average of the wave interactions induces local nonuniformities of the type discussed by Rosa,[9] and allows local DC "Hall currents" to flow internally in the MHD device.

The main results can be summarized by the following equations:

$$E'_{xoo} \cong \Omega_{oo} E'_{yoo} \left\{ 1 - \frac{\langle\!\langle \sigma E'_x \rangle\!\rangle_s - \Omega_{oo} \langle\!\langle \sigma E'_y \rangle\!\rangle_s}{\Omega_{oo} \sigma_{oo} E'_{yoo}} + \frac{\langle\!\langle \sigma \Omega \rangle\!\rangle_s}{\sigma_{oo} \Omega_{oo}} - \frac{2 \langle\!\langle \Omega^2 \rangle\!\rangle_s}{1 + \Omega^2_{oo}} \right.$$

$$\left. + \frac{1}{1 + \Omega^2_{oo}} \left[\frac{\left(1 - \Omega^2_{oo}\right) \langle\!\langle \Omega E'_y \rangle\!\rangle_s + 2\Omega_{oo} \langle\!\langle \Omega E'_x \rangle\!\rangle_s}{\Omega_{oo} E'_{yoo}} \right] \right\}$$

and

$$J_{yoo} \cong \sigma_{oo} E'_{yoo} \left\{ 1 + \frac{\langle\!\langle \sigma E'_y \rangle\!\rangle_s}{\sigma_{oo} E'_{yoo}} - \frac{\Omega^2_{oo}}{1 + \Omega^2_{oo}} \frac{\langle\!\langle \Omega E'_y \rangle\!\rangle_s}{\Omega_{oo} E'_{yoo}} + \frac{\Omega_{oo}}{1 + \Omega^2_{oo}} \frac{\langle\!\langle \Omega E'_x \rangle\!\rangle_s}{\Omega_{oo} E'_{yoo}} - \frac{\langle\!\langle \Omega^2 \rangle\!\rangle_s}{1 + \Omega^2_{oo}} \right\}.$$

In these equations quantities without subscripts represent fluctuations, the angular brackets represent a time average, and $\langle \ \rangle_s$ represents a spatial average. Quantities with double subscript oo are <u>spatial</u> averages of the DC (time-averaged) quantities. For example, if $\hat{j}_y$ is the current density in the y-direction, then $\hat{j}_y = J_{yo} + j_y$, and $\langle \hat{j}_y \rangle \equiv J_{yo}$, $\langle j_y \rangle \equiv 0$, and $\langle J_{yo} \rangle_s \equiv J_{yoo}$. $\hat{\Omega} \equiv \Omega_o + \Omega$ is the local value of $\omega\tau$ in the usual notation, and $\Omega_o \equiv \langle \hat{\Omega} \rangle$. $\underline{\hat{E}}' \equiv \underline{E}'_o + \underline{E}'$ is the electric field in fluid cooridnates.

The coordinate system is so chosen that the y axis lies in the direction of the "desired" current, so that $\left\langle J_{xo} \right\rangle_s \equiv J_{xoo} = 0$, which determines E'_{xoo}. Fluctuations are assumed to be in the plane perpendicular to $\underline{B}_o$, the applied magnetic field, and fluctuations in $\underline{B}_o$ are ignored (low R_m approximation).

When applied to an MHD Faraday-type generator, E'_{xoo} is the maximum DC Hall field that can be developed in the presence of AC fluctuations (other losses being neglected here), and J_{xoo} is the net Hall current, which must vanish in that case.

Application of these results to special cases is discussed in the recent paper.[8] In particular, it is shown how these effects limit the maximum amplitude of fluctuations in an MHD generator subject to a Velikhov instability, and how these fluctuations can be eliminated or controlled by external circuitry.

J. E. McCune

References

1. J. K. Wright, Proc. Phys. Soc. (London) 81, 498 (1963).

2. E. P. Velikhov, Hall Instability of Current-Carrying Slightly Ionized Plasmas, Symposium on Magnetoplasmadynamics, Electrical Power Generation, Newcastle-upon-Tyne, England, September 6-8, 1962.

3. J. E. McCune, Wave Growth and Instability in Partially Ionized Gases, Paper No. 33, International Symposium on MHD Electrical Power Generation, Paris, 1964.

4. J. L. Kerrebrock, AIAA J. 2, 1072 (1964).

5. J. E. McCune, Linear Theory of an MHD Oscillator, Research Report RR 198, AVCO-Everett Research Laboratory, 1964.

6. J. F. Louis, J. Lothrop, and T. R. Brogan, Phys. Fluids 7, 362 (1964).

7. J. Klepeis and R. J. Rosa, Experimental Studies of Strong Hall Effects and V×B Induced Ionization, Research Report RR-177, AVCO-Everett Research Laboratory, 1964.

8. J. E. McCune, Non-Linear Effects of Fluctuations on MHD Performance, paper to be presented at the Sixth Symposium on Engineering Aspects of Magnetohydrodynamics, Pittsburgh, Pennsylvania, April, 1965.

9. R. J. Rosa, Phys. Fluids 5, 1081 (1962).

D. HARTMANN FLOW FRICTION FACTORS — PRESENT AND FUTURE

Considerable time and effort have been expended on the measurement of friction factors in laboratory approximations to Hartmann flow. The purpose of this report is to state what may reasonably be expected from work now under way[1] or planned. There are two main points of interest: the anomalous minimum in f versus M/R curves, and the behavior of f for large M and R. Here, f denotes the friction factor, R the Reynolds number, and M the Hartmann number appropriate to MHD channel flow.

The curves given by Murgatroyd[2] (Figs. XII-6 and XII-7) show that the minimum may disappear at $R \approx 1.2 \times 10^5$. The data of Brouillette and Lykoudis show clearly the

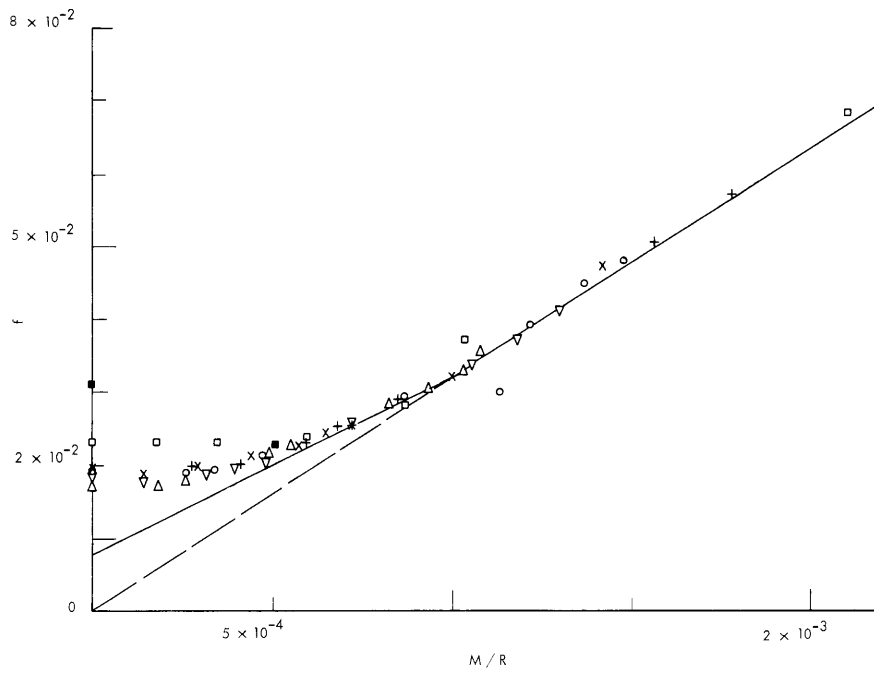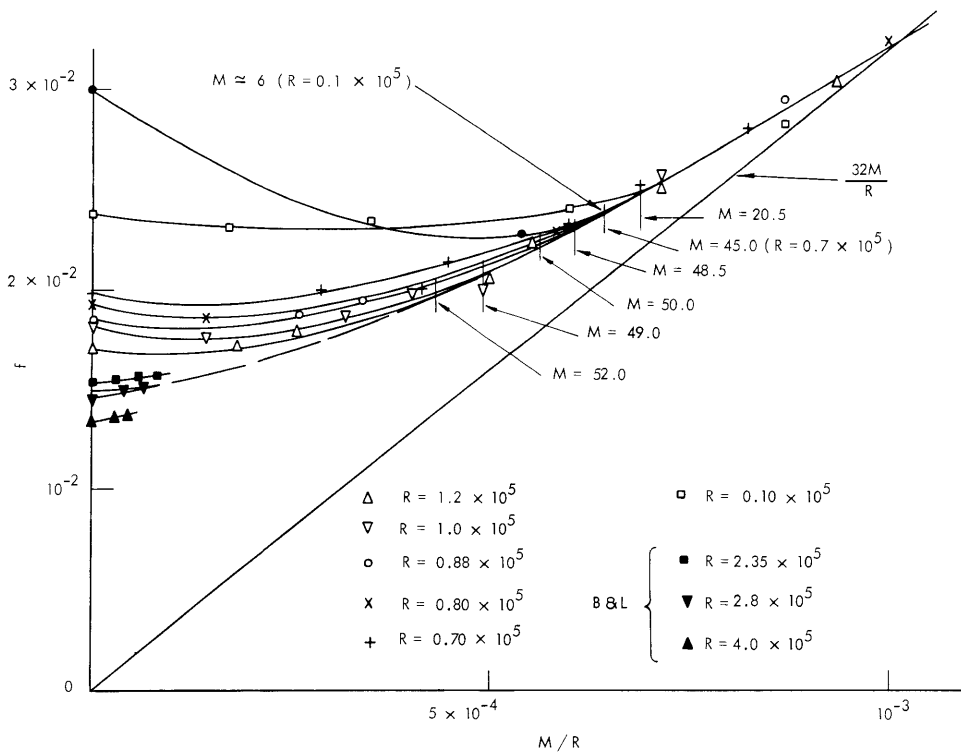Fig. XII-6. f vs M/R from Murgatroyd's curves.

Fig. XII-7. f vs M/R for data of Murgatroyd and of
Brouillette and Lykoudis.

disappearance of this minimum between R = 1.1 × 10^5 and R = 2.3 × 10^5. The latter set of experiments was not conclusive. Harris[4] stated that the minimum occurred at a constant value of $M^2/R*$, which is approximately the line shown in Fig. XII-8. His analysis was based primarily on the data of Murgatroyd, and his conclusion agrees with all of these data very well, with the exception of the curve for highest R (R = 1.2 × 10^5). This one exception (if valid) may be very important. If the trajectory of the minimum in f in the M-R plane (see Fig. XII-8) does turn down for some R, then the minimum may indeed disappear for some R (R > 10^5). The data of Brouillette and Lykoudis, which were not available to Harris, show this turning-down tendency more definitely, although the actual values of M and R are different from Murgatroyd's. Thus, it is possible that an inverted U curve of the type drawn in Fig. XII-8 is the true location of the minimum.
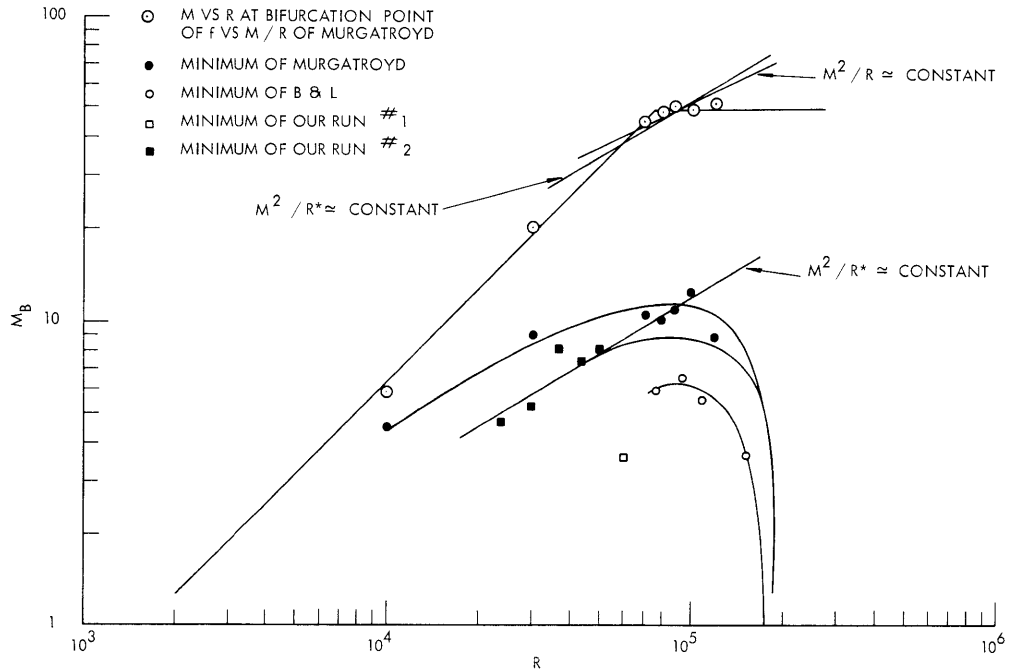

Fig. XII-8. Breakaway value of M vs R.

From the curves of f versus M/R of Murgatroyd (Fig. XII-6) it may be inferred that f = 32 M/R for M/R ≥ 10^{-3}. On a larger scale (Fig. XII-7) the plot shows that an envelope exists for M/R < 10^{-3}, from which curves of f break away at different values of M/R, the value depending on the value of R for which the f vs M/R curve is drawn. On the larger scale plot, the values of M (M_B) at which breakaway occurs are given. For R ≥ 7, 10^4, M_B ≈ 50. The actual values are plotted in Fig. XII-8, and the dependence is found.

$$M_B/R \approx 6.5 \times 10^{-4}, \qquad R \leqslant 7.5 \times 10^4;$$

$$M_B \approx 50, \qquad\qquad 7.5 \times 10^4 \leqslant R \leqslant 1.2 \times 10^5.$$

For $R > 7.5 \times 10^4$, the point at which f begins to be correlated with M/R, generally known as the parameter characterizing laminar flow, is at constant M. This supports the notion that the transition to laminar flow is governed by the boundary-layer thickness. In truly laminar flow, the velocity profile, and also the boundary layer thickness, are functions only of M.

If we extend the envelope assumption, a curve consistent with those drawn, having

$$\left. \frac{\partial f}{\partial M} \right|_{M=0} = 0$$

might be as drawn in Fig. XII-9. This curve has $f(M=0) = 1.5 \times 10^{-2}$, which corresponds to $R \approx 2 \times 10^5$ on standard ordinary hydrodynamic Moody diagrams (f vs R). Thus we might conclude that the anomalous minimum will not be present for $R > 2.0 \times 10^5$.
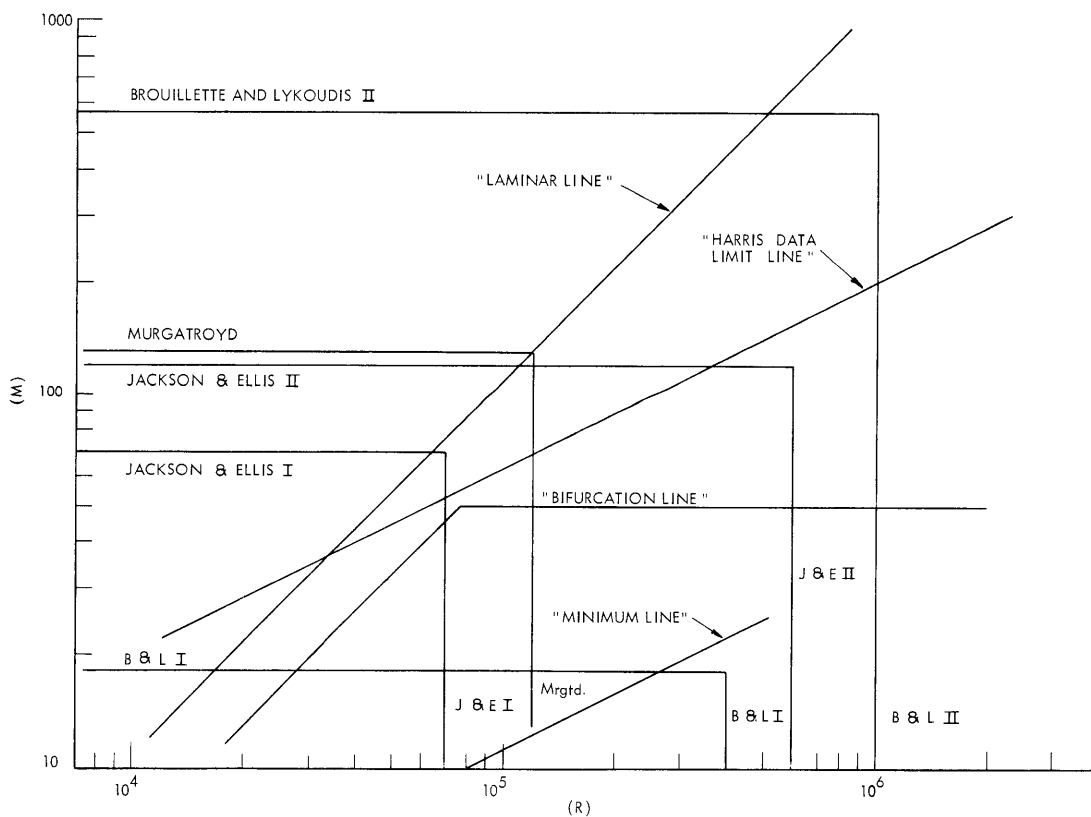

Fig. XII-9. Dependence of f on M^2/R and M/R.

Consider the range of parameters $M^2/R > 4 \times 10^{-2}$, $M/R < 10^{-3}$. Harris predicted that data in this range would be correlated primarily by $M^2/R*$. The breakaway theory, however, predicts that all values of f above and to the left of the "bifurcation line" will be functions of M/R alone. It can be seen that the wedge-shaped region given by the range of parameters considered is completely within the region in which f is a function of M/R alone. Thus data in the range considered may be governed by M/R, rather than by M^2/R or $M^2/R*$.

We propose that the well-known minimum in f versus M/R curves should disappear for $R \gtrsim 2.0 \times 10^5$, provided M^2/R is large. Small values of M/R give little information that cannot be predicted from data now available. If $M > 50$, then any f should be a unique function of M/R in the ranges not yet explored experimentally.

J. R. Ellis, Jr., W. D. Jackson

References

1. W. D. Jackson and J. R. Ellis, Jr., Friction-factor measurements in liquid-metal magnetohydrodynamic channel flows, Quarterly Progress Report No. 73, Research Laboratory of Electronics, M.I.T., April 15, 1964, pp. 122-125.

2. W. Murgatroyd, Experiments on magneto-hydrodynamic channel flow, Phil. Mag. 44, 1348 (1953).

3. E. G. Brouillette and P. S. Lykoudis, Measurements of skin friction for turbulent magnetofluidmechanic channel flow, Purdue Research Foundation Project No. 3093, August 1962.

4. L. P. Harris, Hydromagnetic Channel Flows (Technology Press of M.I.T., Cambridge, Mass., and John Wiley and Sons, Inc., New York, 1960).

E. MAGNETOHYDRODYNAMIC INDUCTION MACHINE WITH LAMINAR FLUID FLOW

In our previous analysis of the MHD induction machine only constant fluid velocity has been considered in illustrating the principles of operation.[1,2] The fluid velocity profile and viscosity will have important effects for two reasons: (i) the velocity profile may drastically alter the power flow; and (ii) the viscous losses may be large. An exact consideration of profile effects is impossible, but a solution can be obtained for laminar flow with reasonable approximations.

The laminar-flow solution gives insight into the mutual interaction. The flow in a practical machine, however, will probably be highly turbulent, because of the high velocities or (hydraulic) Reynolds numbers R_e required to achieve reasonable power densities. Turbulence in induction-driven flows is not fully understood, so that the limits on R_e for laminar flow as a function of the applied magnetic field and flow parameters are unknown. A qualitative idea of turbulence, the turbulent velocity profile, and the effect of

turbulence on machine performance has been obtained,[3] and will be presented in a latter report.

1. Model and Equations

The model to be analyzed is shown in Fig. XII-10. The fluid flows in the x direction between two parallel exciting plates of infinite extent in the x and z directions, spaced 2a apart. The region outside the plates is filled with a core of permeability μ_c and conductivity σ_c. The exciting plates, separated from the fluid and core by insulators of infinitesimal thickness to prevent current flow in the y direction, are assumed to be thin so that they can be replaced by current sheets. The plates are driven by a current source that gives an even or symmetric surface current density

$$\vec{K} = \vec{i}_z NI \cos(\omega t - kx); \tag{1}$$

which represents a traveling current wave of amplitude NI, frequency ω, wavelength $\lambda = \frac{2\pi}{k}$, and velocity $v_s = \frac{\omega}{k}$. The machine of finite length has been treated previously for a constant fluid velocity.[4,5] The extension to include both velocity profiles and finite length is possible for a slit-channel machine because the field solution is independent of the velocity profile for this case only.

The electromagnetic fields are determined from Maxwell's equations with the usual MHD approximation of neglecting displacement currents. The analysis is simplified by the use of a vector potential $\vec{A}$ and scalar potential ϕ defined as

$$\vec{B} = \nabla \times \vec{A} \tag{2}$$

and

$$\vec{E} = -\nabla \phi - \frac{\partial \vec{A}}{\partial t}. \tag{3}$$

Noting that Ohm's law in a moving fluids is $\vec{J} = \sigma(\vec{E} + \vec{v} \times \vec{B})$ and substituting Eqs. 2 and 3 in Maxwell's equations give

$$\nabla^2 \vec{A} - \mu\sigma \frac{\partial \vec{A}}{\partial t} + \mu\sigma(\vec{v} \times \nabla \times \vec{A}) = 0, \tag{4}$$

and

$$\nabla^2 \phi - \mu\sigma \frac{\partial \phi}{\partial t} = 0. \tag{5}$$

Here,

$$\nabla \cdot \vec{A} + \mu\sigma\phi = 0 \tag{6}$$

has been chosen to uncouple Eqs. 4 and 5. The vector potential is due solely to currents, so that it, as well as $\vec{J}$, is in the z direction and independent of z, and $\phi = 0$.
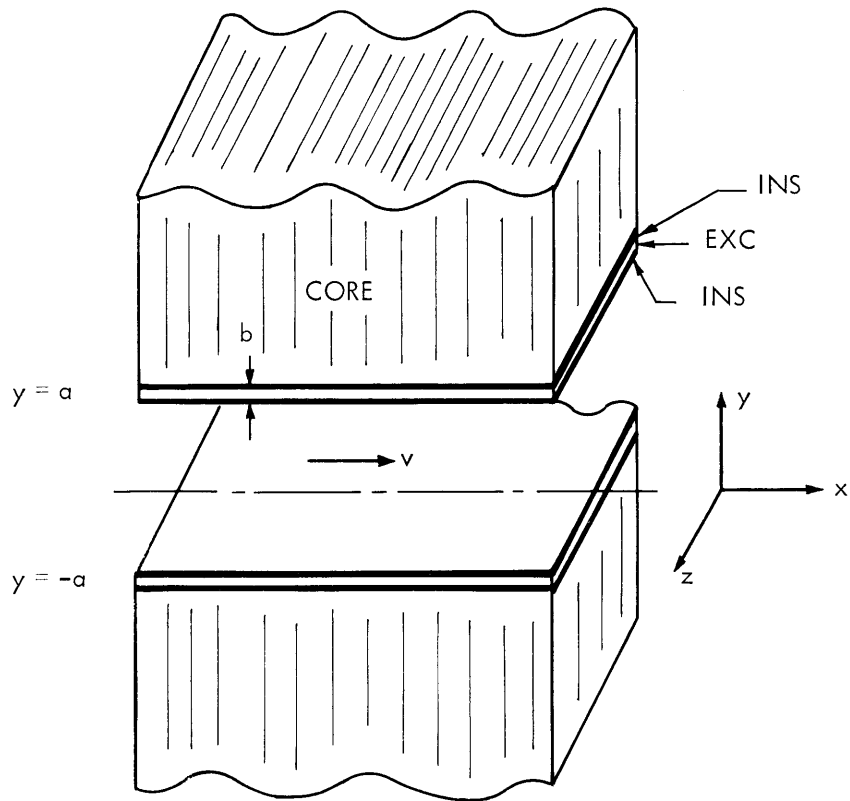
Fig. XII-10. The model.

The fluid behavior is determined from the Navier-Stokes or conservation of momentum equation and the conservation of mass or continuity equation. For an incompressible fluid of mass density ρ and absolute viscosity η, these equations are

$$\rho\left(\frac{\partial}{\partial t}+\vec{v}\cdot\nabla\right)\ \vec{v} = -\nabla p + \eta\nabla^2\vec{v} + \vec{J}_f \times \vec{B}_f, \tag{7}$$

and

$$\nabla \cdot \vec{v} = 0, \tag{8}$$

where p is the pressure, subscripts f and c denote fluid and core quantities, and $\vec{J}_f$ and $\vec{B}_f$ can be expressed in terms of $\vec{A}_f$.

The equations can be solved only for laminar flow, as little is known about solutions for turbulent flows either with or without a magnetic field. Even then, an analytical solution is clearly impossible, because of the nonlinear terms and the two-directional coupling, so that a reasonable approximation is made — that the fluid velocity is laminar, in the x direction, and independent of x and t. This approximation and the resulting equations are discussed below. An analytical solution of the simplified equations is

obtained for a slit channel. In general, even the simplified equations can only be solved numerically because the nonlinear terms and the two-directional coupling remain. The numerical techniques and results are also discussed.

2. Approximate Equations for Laminar Flow

To solve Eqs. 4 and 7, they must be simplified, because of the product type of non-linearities. Linearization with the constant-velocity solution used as the starting point is not valid for two reasons: the constant velocity does not match the boundary conditions, and the perturbations are not small. A power-series solution in the magnetic Reynolds number $R_M = \mu_f \sigma_f v_s / k$ is not desired because it would be limited to small R_M, which does not include the range of interest for power generation. Writing $\vec{v}$ and $\vec{A}_f$ as Fourier series in $e^{jn(\omega t - kx)}$, because of the simple $e^{j(\omega t - kx)}$ excitation of the current sheets, gives an infinite number of completely coupled equations that still involve products and derivatives with respect to y. These equations are not amenable to solution.

The equations are simplified by assuming the velocity to be completely in the x direction. The continuity equation then requires $\vec{v}$ to be independent of x. The electromagnetic pressure gradient on each strip, $(\vec{J}_f \times \vec{B}_f)_x$, consists of a constant term plus a second harmonic in $(\omega t - kx)$, since $\vec{J}_f$ and $\vec{B}_f$ vary as $e^{j(\omega t - kx)}$ for a velocity independent of x and t. The total force on a strip per wavelength in the x direction is a constant, so that v should not have any time dependence for an incompressible fluid. Thus, $\vec{v} = \vec{i}_z v(y)$ is a consistent and reasonable approximation to the actual flow, provided the transverse fluid velocity is small compared with the velocity along the machine. This can be justified for a slit-channel machine by examining the driving forces.[6]

The equations are put in a more tractable form by using complex notation, $\vec{A}_f(x,y,t) = R_e\left\{\vec{i}_z \underline{A}_f(y)\, e^{j(\omega t - kx)}\right\}$, and by defining the normalized variables $\tilde{y} = \dfrac{y}{a}$, $u(\tilde{y}) = \dfrac{v(\tilde{y})}{\bar{v}}$, and $F(\tilde{y}) = \dfrac{\underline{A}_f(\tilde{y})}{\underline{A}_{fo}}$, where a is the channel half-height, $\bar{v}$ is the average velocity, and $\underline{A}_{fo}$, the vector potential at the center of the channel, is determined by the boundary conditions. In terms of v_s and the average slip $\bar{s}$, $\bar{v} = (1-\bar{s})v_s$, which is considered to be a constant of the solution.

The Hartmann number for DC flows is

$$M_o^2 = \frac{\sigma_f a^2}{\eta} B_o^2, \tag{9}$$

where B_o is the transverse magnetic field. If we define an effective Hartmann number $M(\tilde{y})$ for the induction machine,

$$M^2 = \frac{\sigma_f a^2}{\eta} \frac{A_f A_f^*}{2},$$

(10)

in terms of the rms transverse magnetic field, where a = ak, the normalized equations become

$$\frac{d^2 \underline{F}}{d\tilde{y}^2} - a^2 [1+jR_M-jR_M(1-\bar{s})u] \underline{F} = 0,$$

(11)

and

$$\frac{d^2 u}{d\tilde{y}^2} - M^2 u = \frac{a^2 P_o}{\eta(1-\bar{s}) v_s} - \frac{M^2}{(1-\bar{s})}$$

(12)

from Eq. 4 and the space or time average of Eq. 7. Equation 12 is identical to the Hartmann profile equation for a DC generator in terms of a proper loading factor.

The original set of equations has been simplified to two coupled nonlinear ordinary differential equations. An analytical solution, possible only for a slit channel, is given below. The general case is also treated numerically. The solution could be obtained by series techniques, but these are of limited validity.[7] Also, the present approach is easier to use and more flexible.

The electromagnetic powers can be written in terms of the normalized variables, but the simple power relations[1,8] no longer exist. In general, the magnitudes of P_m and P_r, the mechanical power output and the power dissipated in the fluid because of its finite conductivity, are increased over their constant-velocity values for a generator, because of the circulating currents that are set up, since the velocity drops below synchronous speed near the walls. This region acts as a pump, and the net behavior of the machine may be changed from a generator to a pump or damper.

3. Slit-Channel Solution

For a slit channel, $\gamma a \ll 1$, the equations can be simplified to yield analytical solutions. The electromagnetic field and the vector potential are independent of y, and the total current in the field at a given value of x is therefore independent of the velocity profile. This means that the vector potential can be determined first, and then the profile and powers. The vector potential, depending only on the total current, is the same as the slit-channel field that is found for a constant velocity,

$$A_f = \frac{\mu_f NI}{k(\gamma^2 a + \kappa \delta)},$$

(13)

where $\gamma^2 = 1 + jsR_M$, $\kappa = \frac{\mu_f}{\mu_c}$, and $\delta^2 = 1 + j\frac{\mu_c \sigma_c v_s}{k}$.

The velocity, obtained from Eq. 12 for M constant, is the Hartmann profile,

$$u(\tilde{y}) = \frac{\left(1 - \dfrac{\cosh M\tilde{y}}{\cosh M}\right)}{\left(1 - \dfrac{\tanh M}{M}\right)};$$

(14)

so that, for a slit channel and laminar flow, the profile for the induction machine is identical to that for a DC machine with a Hartmann number based on the rms transverse magnetic field. The Hartmann profile is plotted in Fig. XII-11 for several values of M. The curve for M = 0 is the parabolic profile of laminar hydrodynamic flow.

The powers for the slit-channel machine[1,8] are

$$P_s = P_o \frac{a \bar{s} R_M}{(\gamma^2 a + \kappa \delta)(\gamma^{*2} a + \kappa \delta^*)},$$

(15)

$$P_m = (1 - \bar{s}) P_s F_m(u),$$

(16)

and

$$P_r = \bar{s} P_s F_r(u),$$

(17)

where $P_o = \mu_f v_s N^2 I^2 c\ell$, and c and ℓ are the machine length and width. Here P_s, the time-average real power supplied to the fluid, is independent of the profile, since it depends only on the fields. The equations are identical with the results for constant fluid velocity except for the profile factors

$$F_m(u) = \frac{1}{\bar{s}}\left[1 - (1 - \bar{s})\overline{u^2}\right],$$

(18)

and

$$F_r(u) = \frac{1}{\bar{s}^2}\left[2\bar{s} - 1 + (1 - \bar{s})^2 \overline{u^2}\right],$$

(19)

where

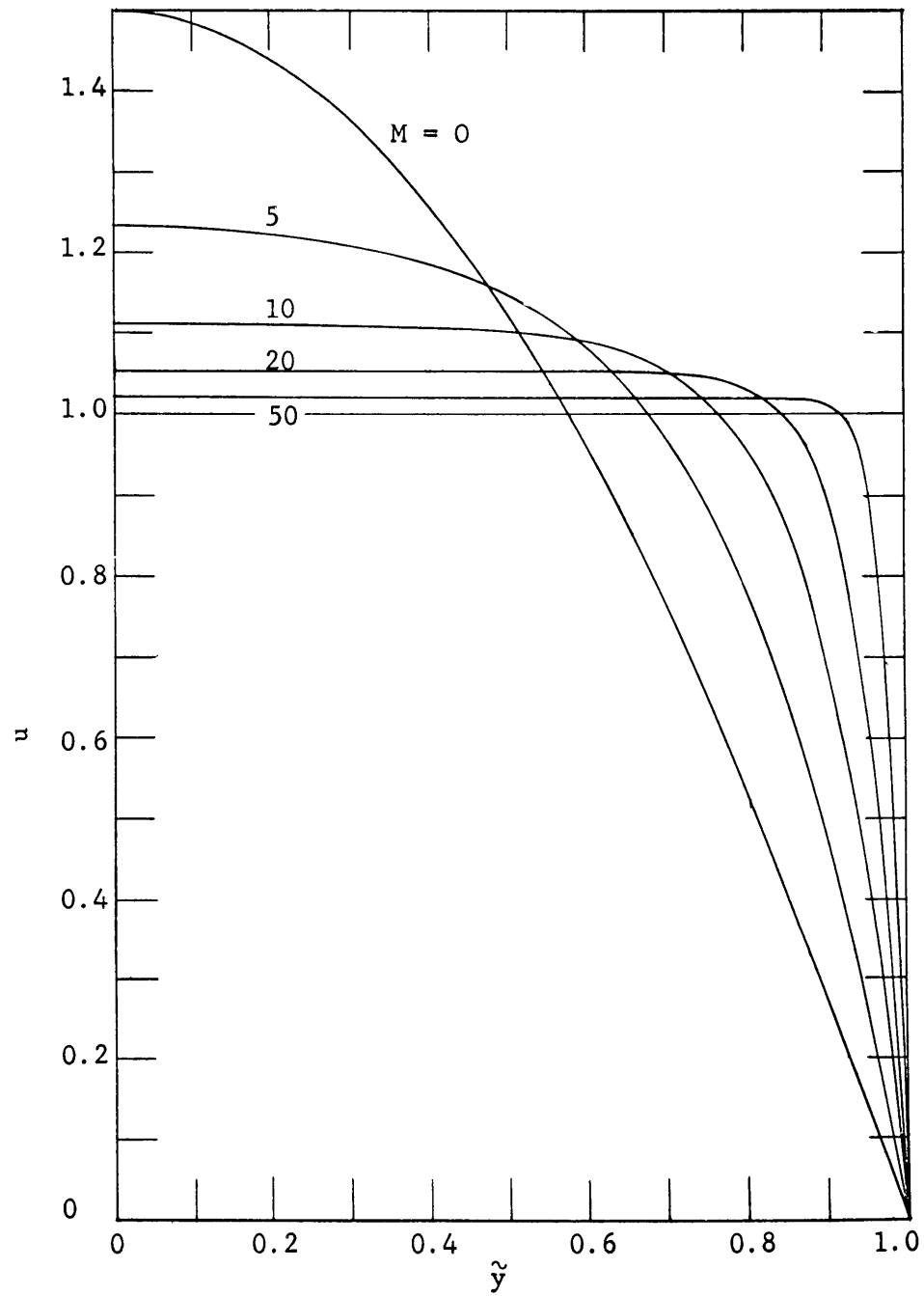$$\overline{u^2} = \int_0^1 (u(\tilde{y}))^2 \, d\tilde{y},$$

(20)

Fig. XII-11. Normalized Hartmann velocity profiles.

the average of the velocity squared, is always ≥ 1. For a generator, F_m and F_r are ≥ 1, and the $I^2 R$ losses are increased for the same power output. For a pump, $F_m \leq 1$.
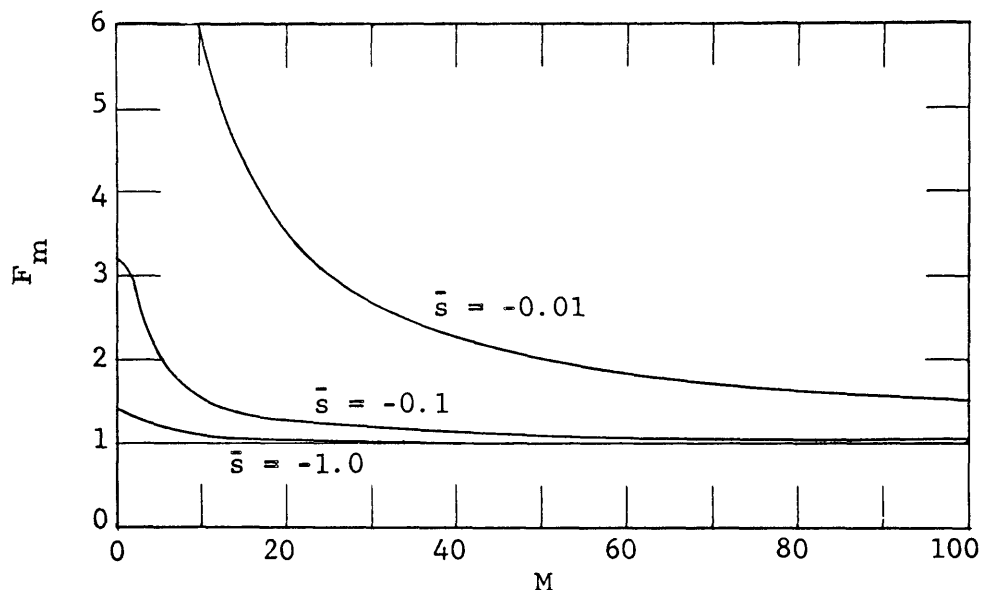

Fig. XII-12. F_m for Hartmann profile.

The profile factors for a Hartmann profile, plotted in Figs. XII-12 and XII-13 for several negative values for $\bar{s}$, show that the factors increase as $|\bar{s}|$ decreases and as the profile deviates from a constant. This is to be expected for a generator because, as $\bar{s}$ approaches zero or as the profile becomes more rounded, the size and relative importance of the positive-slip region near the wall increases. In this region the machine is acting as a pump, so that the losses resulting from circulating currents are increased.

The generator efficiency, P_s/P_m, is

$$e_g = \frac{1}{(1-\bar{s})F_m},$$

(21)

since P_s is unchanged but the input power is increased by F_m. At $\bar{s} = 0$, there is no power output, but the circulating currents still exist, there is power input, and the efficiency is zero. There is a peak in the efficiency, so that decreasing $|\bar{s}|$ further results in a poorer efficiency because more of the fluid is pumped, in contrast to the constant-velocity case for which e_g approached one as $\bar{s}$ approaches zero. Curves of e_g versus $\bar{s}$ for several values of M are shown in Fig. XII-14.

These results, derived by assuming $\gamma a \ll 1$, are valid for a much larger range than
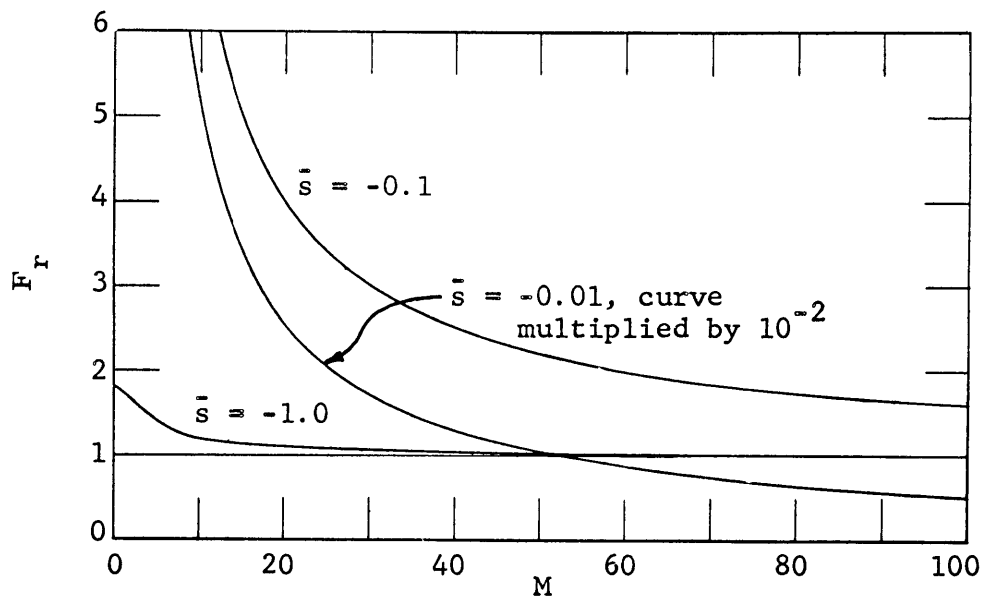
Fig. XII-13. F_r for Hartmann profile.

expected. Comparison with the numerical results shows good agreement for a as large as 0.1; that is, errors of a few per cent for $a = 0.1$ and $|\bar{s}R_M|$ up to 100.
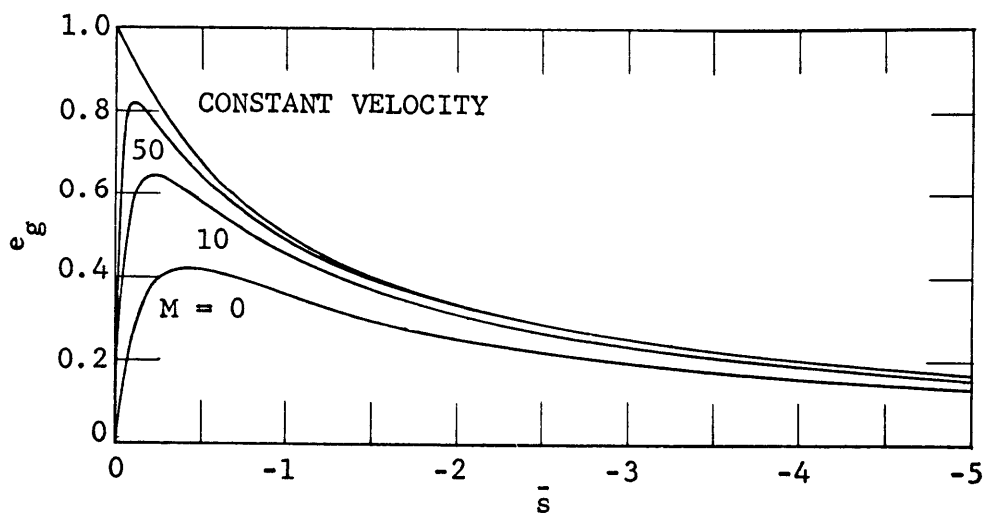

Fig. XII-14. Generator efficiency for slit-channel machine with Hartmann profile.

4. An Iterative Solution

The vector potential in the fluid can be determined from Eq. 11 when the velocity is specified. The result when the profile for ordinary hydrodynamic flow, either laminar

or turbulent, is used is the approximate solution when the electromagnetic force is small compared with the viscous force. Otherwise, the result may not correspond to an actual flow, but still gives information on the dependence of the fields and powers on the velocity profile. Equation 11 is a linear homogeneous second-order differential equation for $\tilde{F}(\tilde{y})$ in terms of $u(\tilde{y})$ and the machine parameters. Several numerical methods were used to solve Eq. 11 when the velocity was specified, and the preferred method was chosen by testing on the case $u(\tilde{y}) = 1$, for which the exact solution is known. The numerical integration procedure for Eq. 11 worked quite well.[9]

Equation 12 can be solved for the fluid velocity profile when the vector potential is specified. The profile obtained is the small sR_M solution if the field with no fluid present is used, corresponding to the case for which the field is not appreciably affected by the fluid. The solution of the nonhomogeneous Eq. 12 is more complicated than the solution of the homogeneous Eq. 11. Before, there was only a homogeneous solution for specified initial conditions, which was scaled to match the boundary conditions. Now, there is a homogeneous solution and one or two particular solutions, which depend on the approach used. Initial conditions are specified, and then a linear combination of the solutions is used to match the boundary conditions. Several approaches to solving Eq. 11 were tested. Difficulty occurred, because of the exponential-like behavior of the solutions, which could not be avoided. This puts a limit on the parameters for which the solution can be obtained.[10]

The techniques developed for solving Eqs. 11 and 12 can be combined to obtain an exact solution for laminar flow by iterating. The electromagnetic field for a constant fluid velocity is used as the starting point, and Eqs. 12 and 11 are solved repetitively for the new velocity and field in that order, until the solution converges to the desired accuracy. The convergence is good for R_M small, but becomes worse as R_M increases because the fluid profile has more effect on the field.

All the $\alpha = 0.1$ cases tested with the iterative procedure checked with the slit-channel results, except for $sR_M = -250$, where M^2 varied by a factor of three across the channel, and the profile was no longer Hartmann. The small $\gamma\alpha$ case is excluded from further consideration here as it is better treated by the methods discussed in section 3.

Some of the results for large $\gamma\alpha$ are given in Figs. XII-15, XII-16, XII-17, and in Table XII-1. The number of iterations required for convergence to five figures is given in Table XII-1, where > means that the result is close, but more than the number tried were required. The number increases with increasing $\bar{s}$ and R_M. The excitation magnitude is contained in the normalization constant $FOR = \mu_f(NI)^2 a/2\eta v_s$.

The velocity profiles for $\alpha = 1$, $R_M = 1$ and 10, are plotted in Figs. XII-15 and XII-16 for $\bar{s} = -0.1$, -1, and -10. The two $\bar{s} = -0.1$ curves look similar, but are quite different near the walls. The power density and efficiency for $\bar{s} = -10$ are greater than for a
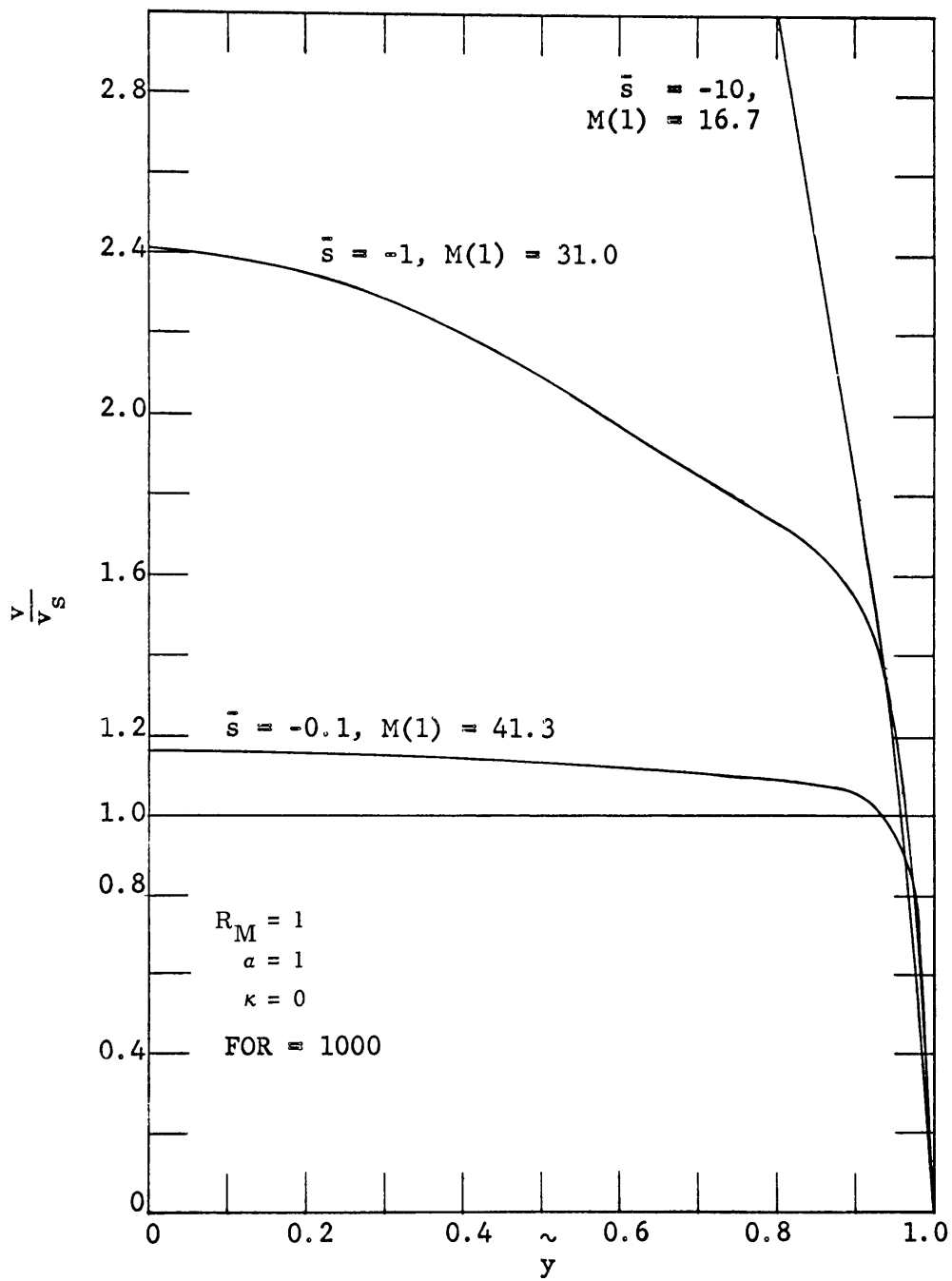
Fig. XII-15. Iterative solution for velocity, $a = 1$,
$R_M = 1$, FOR = 1000.

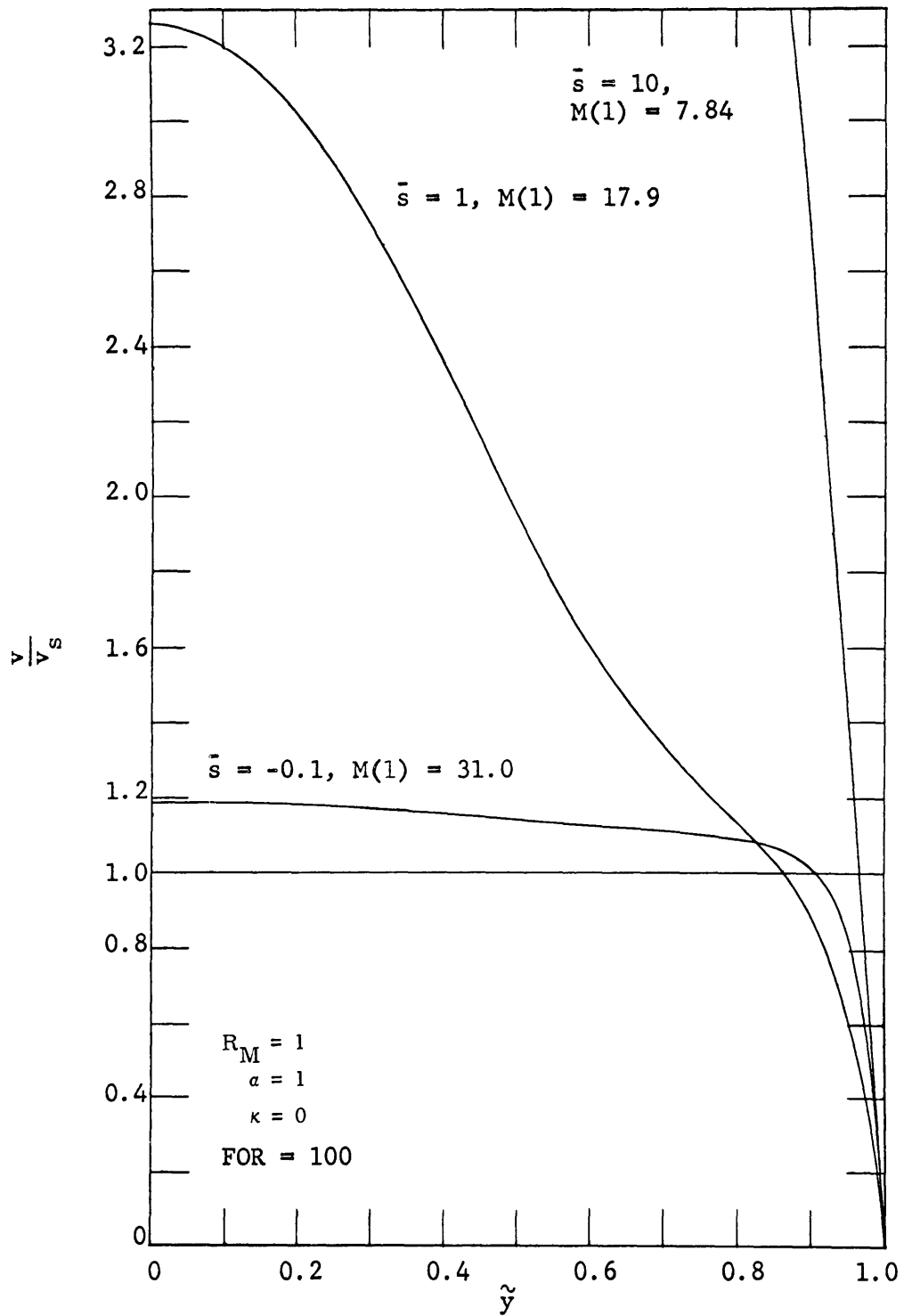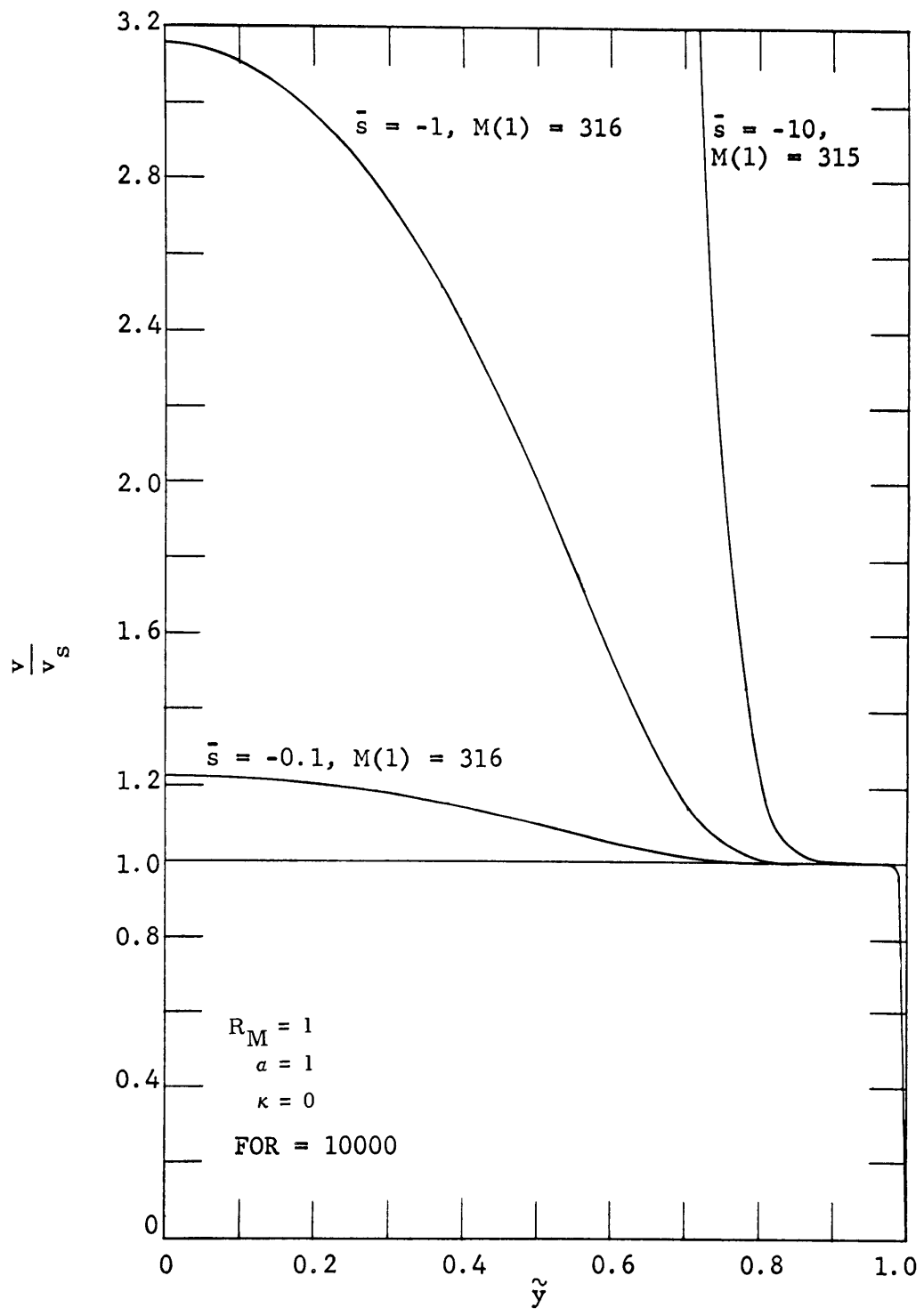Fig. XII-16. Iterative solution for velocity, $a = 1$, $R_M = 10$, FOR = 100.

Fig. XII-17.   Iterative solution for velocity, $a = 10$, $R_M = 1$, FOR = 10,000.

constant fluid velocity because the average slip seen by the field is less than the average for the fluid. This is not of practical significance because the power density and efficiency are both low.

The profiles for $a = 10$ and $R_M = 1$, show the strong field influence at the wall. The electromagnetic dominance is more pronounced for larger excitation and extends farther

Table XII-1. Iterative solution results, $\kappa = 0$.

$\bar{s}$	R_M	a	FOR	M(1)	$\dfrac{P_s}{P_o}$	e_g, %	Required number of iterations
-0.1	1	1	1000	41.3	-0.0753	69.9	2
-1				31.0	-0.456	47.1	4
-10				16.7	-0.168	10.3	>5
-0.1	10	1	100	31.0	-0.287	57.3	>3
-1				17.9	-0.0388	13.8	>5
-10				7.84	-0.0957	17.8	>5
-0.1	1	10	1000	99.5	0.0937	Pump	2
-1				99.5	0.0885	Pump	5
-10				97.2	0.0443	Damper	>6
-0.1	1	10	10,000	316	0.0310	Pump	3
-1				316	0.0302	Pump	5
-10				315	0.0238	Damper	>5

into the fluid. None of the tested $a = 10$ cases will operate as a generator, since the pumping of the boundary layer dominates, as shown in Table XII-1.

The exact solution has been obtained for several sets of parameters, and can be extended to others if desired. One important result is to eliminate the large γa machine from further consideration. Not only is the power density low, but it will not operate as a generator. The slit-channel results have been used to obtain predicted performance characteristics.[11]

E. S. Pierson, W. D. Jackson

References

1. E. S. Pierson, Power flow in the magnetohydrodynamic induction machine, Quarterly Progress Report No. 68, Research Laboratory of Electronics, M.I.T., January 15, 1963, pp. 113-119.

2. W. D. Jackson, E. S. Pierson, and R. P. Porter, Design Considerations for MHD Induction Generators, International Symposium on Magnetohydrodynamic Electrical Power Generation, Paris, July 6-11, 1964.

3. E. S. Pierson, The MHD Induction Machine, Sc. D. Thesis, Department of Electrical Engineering, M. I. T., Cambridge, Massachusetts, 1964; see Chap. 5.

4. Ibid., Chap. 6.

5. E. S. Pierson and W. D. Jackson, Magnetohydrodynamic induction machine of finite length, Quarterly Progress Report No. 75, Research Laboratory of Electronics, M. I. T., October 15, 1964, pp. 92-103.

6. E. S. Pierson, Sc. D. Thesis, op. cit., pp. 76-78.

7. J. P. Penhune, Energy Conversion in Laminar Magnetohydrodynamic Channel Flow, ASD Technical Report 61-294, Research Laboratory of Electronics, M. I. T., August 1961, pp. 75-78.

8. E. S. Pierson, The MHD Induction Machine, Sc. D. Thesis, op. cit., Sec. 3. 3.

9. Ibid., Sec. 4. 4.

10. Ibid., Sec. 4. 5.

11. E. S. Pierson and W. D. Jackson, Prediction of magnetohydrodynamic induction generator performance, Quarterly Progress Report No. 76, Research Laboratory of Electronics, M. I. T., January 15, 1965, pp. 156-164.

F. BEHAVIOR OF DRY POTASSIUM VAPOR IN ELECTRIC AND MAGNETIC FIELDS

A description of preliminary measurements of the electrical properties of wet and dry potassium vapor was given in Quarterly Progress Report No. 74 (pages 155-166). These results have also been reported in detail.[1]

Although the results for nonequilibrium conduction in wet vapor appeared to be consistent with theoretical predictions, those for the dry vapor were confusing. In particular, the measured electrical conductivities in the nonequilibrium regime were as much as a factor of ten larger than those expected from theory.

More refined measurements of the conductivity of the dry vapor have now been carried out, both with and without a magnetic field. The present discussion is a preliminary report of these results.

1. Apparatus

The most important modifications to the experimental facility are indicated schematically in Fig.XII-18. Whereas in the earlier experiments[1] the best section was located in the condenser and electrical connections were taken out through the condenser, the test section is now located in an argon-purged vacuum enclosure below the condenser. This new arrangement has the advantage of making the test leads more accessible and perhaps less susceptible to shorting. It has the disadvantage that many joints between the electrical insulator and the metal parts must be made gas tight.

In the present design the boron-nitride test-section tube is joined to the metal parts by tapered joints as shown in Fig. XII-18. The probes are held in stainless-steel taper pins. This design was not as leak-tight as we desired, but it was adequate to produce some data.

An electric field was imposed on the plasma by means of the electrodes at the top and bottom of the test section. A magnetic field was imposed in a direction perpendicular to the tube axis (and to the electric field). This combination leads to a Hall field
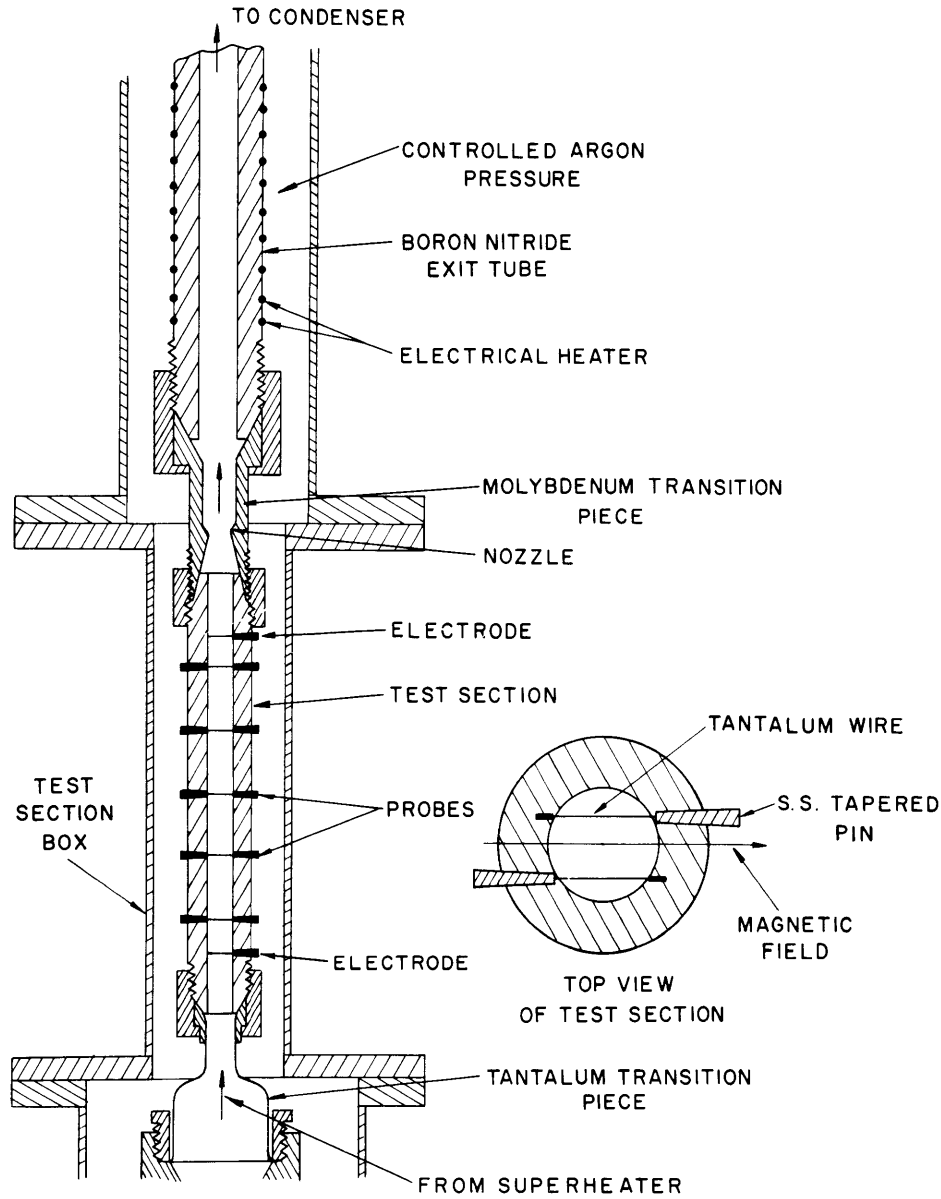

Fig. XII-18. Test section assembly.

normal to both, which was measured by means of the pairs of probes shown schematically at the right in Fig. XII-18. In order to prevent shorting of the test section through ground at its two ends, a long (approximately 1 ft) insulating exit tube was placed between

the test section and condenser. Both the test section and the exit tube were heated to prevent condensation.

A throat, located downstream of the test section, was sized to give a Mach number of 0. 6 in the test section.

2. Experimental Results

The experimental results consist of axial and transverse voltages, as functions of the axial current and the magnetic field.

In Fig. XII-19 the variation of voltage along the test section is given as a function of the current density, for zero magnetic field. The curves are linear; this indicates that
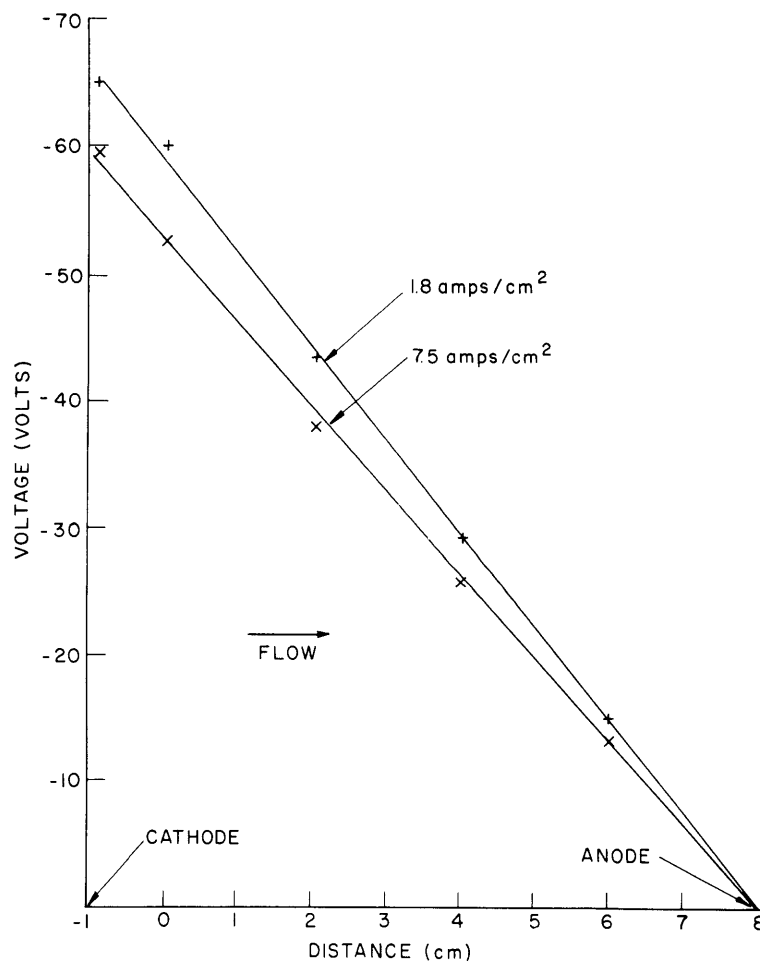

Fig. XII-19. Voltage distribution along channel for various current densities, and zero magnetic field.

a nearly constant conductivity was attained in the plasma.

From these and other similar results, the plasma conductivity was determined as a

function of the current density. The results are compared with the two-temperature theory[2] in Fig. XII-20. Two theoretical curves are given to indicate the uncertainty in plasma pressure and temperature. The spread of the data is indicated by the bars, and the mean of several point by the circles. We conclude that, within the uncertainty in the plasma conditions, the measured conductivity agrees with that predicted theoretically. In the light of current understanding of two-temperature plasmas, this may be interpreted to mean that the electron collision cross section of potassium is 250×10^{-16} cm^2 within approximately 15 per cent.
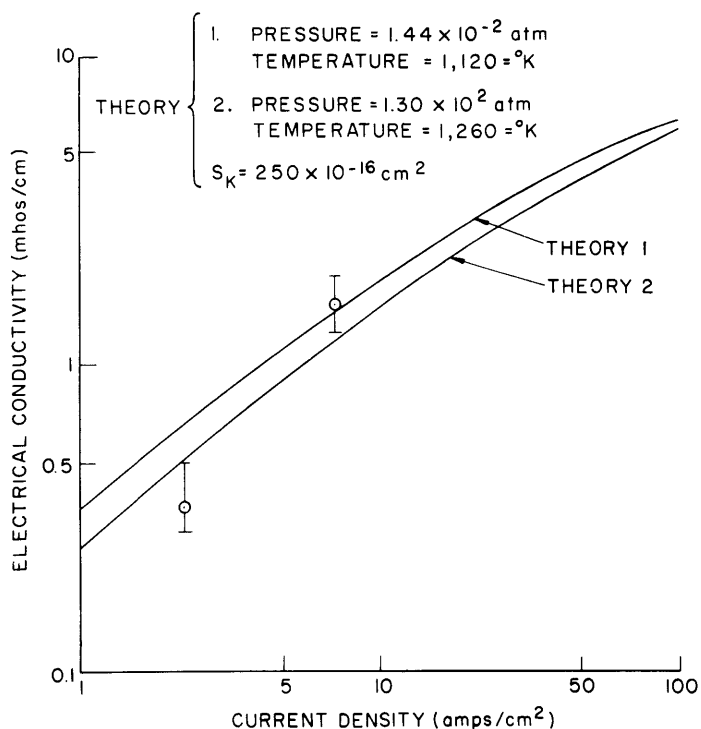

Fig. XII-20. Nonequilibrium electrical conductivity of pure superheated potassium vapor.

Further confirmation of this value is offered by the measurements of Hall voltage. We note first of all that if the axial and transverse directions are denoted z and y, respectively, while the magnetic field is in the x direction, the current densities are given by

$$j_z = \sigma E_z + \beta j_y \tag{1}$$

$$j_y = \sigma E_y + \beta (j_o - j_z), \tag{2}$$

where σ is the local conductivity, β is the local Hall parameter, and $j_O = en_e V$, with n_e being the local electron density and V the flow velocity.

Now, if $j_y = 0$, then $j_z = \sigma E_z$, and

$$\frac{E_y}{E_z} = \beta \left(1 - \frac{j_O}{j_z} \right).$$

(3)

Having j_O and j_z, we can therefore deduce a value of β from the measured E_y and E_z. Such results are shown as the triangular points in Fig. XII-20. There is a great deal of scatter, and considerable systematic deviation from the theoretical result based on the cross section of 250×10^{-16} cm^2.

In fact, j_y is not exactly zero, because of local shorting of the Hall voltage by non-uniformities and by the probes. But if we define an effective conductivity,

$$\sigma_{eff} = \frac{j_z}{E_z},$$

(4)

we have from Eq. 1,

$$1 = \frac{\sigma}{\sigma_{eff}} + \beta \frac{j_y}{j_z} = \frac{\sigma}{\sigma_{eff}} + \beta \left[\frac{\sigma}{\sigma_{eff}} \frac{E_y}{E_z} - \beta \left(1 - \frac{j_O}{j_z} \right) \right].$$

Let $\beta_{eff} = E_y/E_z (1 - j_O/j_z)$, and set $s = \sigma_{eff}/\sigma$ and $b = \beta/\beta_{eff}$. Then

$$1 - \frac{1}{s} = \beta \left(1 - \frac{j_O}{j_z} \right) \left[\frac{\beta_{eff}}{s} - \beta \right] = \beta_{eff}^2 \left(1 - \frac{j_O}{j_z} \right) \left[\frac{b}{s} - b^2 \right].$$

Solving for b, we find

$$b = \left\{ \frac{1}{2} + \sqrt{\frac{1}{4} - \frac{(s-1)s}{\left(1 - \frac{j_O}{j_z} \right) \beta_{eff}^2}} \right\} \frac{1}{s}.$$

Now taking $s = \sigma_{eff}/\sigma$ as the ratio of σ_{eff} to the σ determined experimentally for B = 0, and evaluating $1 - j_O/j_z$ similarly from the experimental results for B = 0, we can compute b, and hence the actual value of β. The data corrected in this way are shown as the circles in Fig. XII-21. They agree quite well with the theoretical results. We conclude
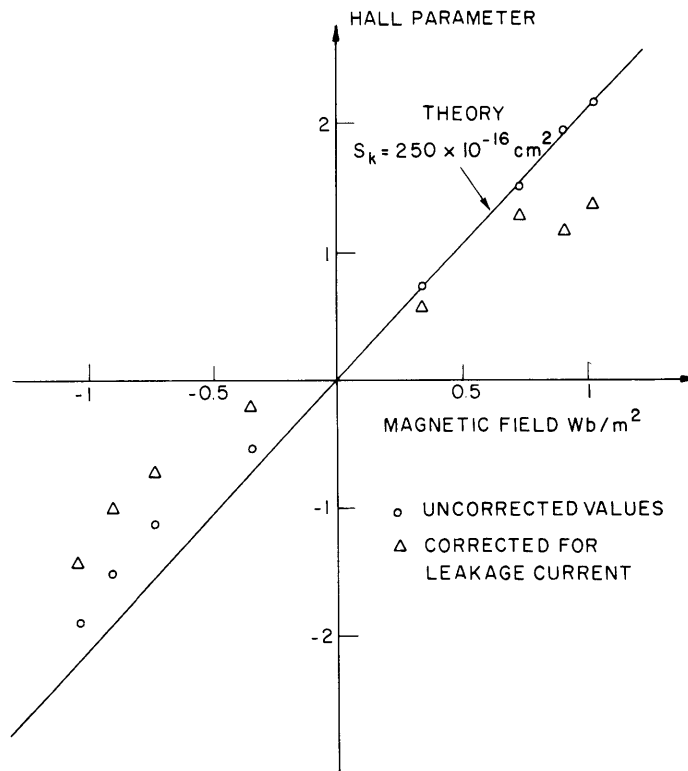
Fig. XII-21. Hall parameter versus magnetic field. (Triangles represent the meas-
ured Hall field; circles are corrected for Hall field shorting.)

that β and σ are essentially constant, and that the deviation of the measured Hall fields
from the expected value is due to shorting of the Hall fields by the probes, by the inlet
and outlet nozzles or, perhaps, by the walls.

3. Conclusions

To summarize, we conclude that, within the accuracy of this experiment, the
electric conductivity of dry potassium vapor is as predicted by the two-temperature
theory.[2]

The conductivity measurements for zero magnetic field and Hall field measurements
at Hall parameters up to 2 indicate independently an electron collision cross section
of 250×10^{-16} within 15 per cent.

J. L. Kerrebrock, M. A. Hoffman, A. Solbes

References

1. A. W. Rowe and J. L. Kerrebrock, Nonequilibrium Electric Conductivity of Wet
and Dry Potassium Vapor, Technical Documentary Report No. APL-TDR-64-106,
Research Laboratory of Electronics, Massachusetts Institute of Technology, Cambridge,
Massachusetts, November 2, 1964.

2. J. L. Kerrebrock, Nonequilibrium Ionization Due to Electron Heating: I. Theory,
AIAA J. 2, 1072-1080 (1964).

G. BONDING MECHANISM OF ALKALI-METAL ATOMS ADSORBED ON METAL SURFACES

1. Introduction

Several illuminating theoretical studies of surface and adsorption phenomena of metal vapors on dissimilar metal substrates have been published.[1-3] An interesting point is that each treatment proposes an entirely different physical mechanism for cesium adsorption on metals. Despite this seeming variance, all three theories are able to explain experimental data relevant to cesium adsorption. These data consist of experimentally measured thermionic electron emission from cesiated surfaces and energies of adsorption of the cesium.

At this point a brief summary of the salient features of each of these analyses is in order. Gyftopoulos and Levine[1] propose that cesium is chemisorbed on the surface thereby forming a partially ionic-partially covalent bond with the four substrate atoms upon which the cesium rests, thereby forming essentially a CsW_4 molecule lying on the surface. To a large extent, they neglect the effects of the other substrate atoms. Their results agree well with experiment.

Gomer and Swanson[2] attempted a semiquantitative study to obtain knowledge of the basic physical mechanism giving rise to energies of adsorption. They feel that as an alkali atom such as cesium (in which the outer shell electron-energy level lies above the Fermi level) is brought to a metal surface, this level becomes greatly broadened. This broadening, which is analogous to natural broadening in plasmas, stems from the fact that the atom, brought into an interacting state with the metal, has a finite lifetime as an atom, and thus an uncertainty in its energy according to the uncertainty principle. They feel that the 6s level of cesium is broadened so greatly (several electron volts) that the atom level overlaps the conduction band of the substrate. It is then possible for polar metallic bonds to form between adsorbate and substrate. This can occur only if there is significant overlap of the broadened atomic level and the conduction band of the substrate.

Rasor and Warner[3] feel that cesium adsorption can be treated as if distinct species of atom and ions exist on the surface. The ratio of atoms and ions is obtained through a statistical mechanical treatment. For cesium on refractory metals at temperatures of 1000°K most of the adsorbates are ions. Those ion adsorbates are bonded to the surface by purely ionic bonds. They justify this by arguments that include the necessity for the atomic level to be unbroadened. Through rough and questionable calculation they conclude that the level is broadened much less than 0.2 ev and thus their model is valid.

In this report, the high points of a detailed investigation[4] into the nature of the cesium-substrate bond are presented. Some of the ambiguity and confusion resulting from the differences summarized above will be removed. Detailed mathematics will be
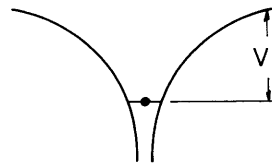
Fig. XII-22. Sommerfeld metal.
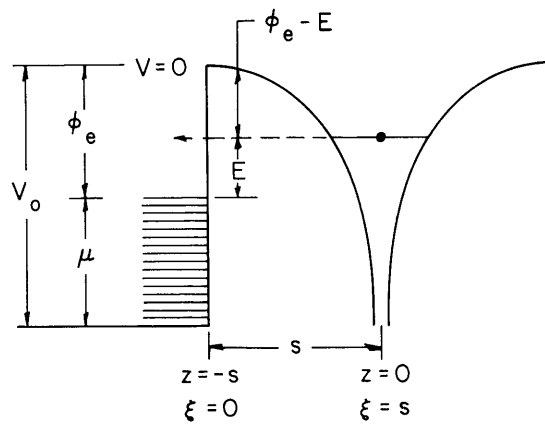

Fig. XII-23. Isolated atom.

Fig. XII-24. Interacting metal and atom.

omitted, since it can be found elsewhere.[4] Only the basic physics and terminal results are reported herein.

2. Physical Model

The metal upon which cesium is adsorbed is considered to be a Sommerfeld metal. This is shown in Fig. XII-22. The isolated atom is shown in Fig. XII-23. In this figure, μ is the height of the zero temperature Fermi level; ϕ_e, the electron work function of the metal; and V_i, the unperturbed ionization potential of cesium.

As the atom at a distance s from the surface is allowed to interact with the metal, Fig. XII-24 may be considered. The dashed line indicates the transition of the electron from the atom to the metal; Z and ξ are simply coordinates; and E is defined by the figure in which $\phi_e - E$ is the perturbed ionization potential of the atom. Hagstrum[5] has shown both theoretically and experimentally that the conduction band of the metal retains all of its bulk properties out to the surface, so Fig. XII-24 is valid. Thus the idea of the CsW_4 molecule seems incorrect. Since the detailed nature of the surface barrier does not enter the ensuing calculations, the fact that a square well has been drawn in Fig. XII-24 is of no consequence.

3. Transition Process

As an atom is brought to a metal surface and is allowed to interact with the metal, the outer electron will want to make transitions into other energetically permissible quantum states such as are in the metal. If there is a perturbation coupling the two states, the transition probability can be determined. Calculations somewhat analogous to the work presented here have been made for Auger neutralization of ions by metals.[5-7]

The transition probability per unit time is given by the "Golden Rule" as

$$w = \frac{2\pi}{\hbar} \int |\langle \psi_m | H' | \psi_a \rangle|^2 \, \rho_k \, d\Omega \tag{1}$$

with ψ_m the final-state metal wave function; ψ_a the initial-state atom wave function; H' the perturbation mixing the two states; ρ_k the density of final states; and the integration performed over all directions of K in the final state.

For a Sommerfeld metal the following wave functions result:

$$\psi_m = \frac{1}{K_v L^{3/2}} \exp[i(K_{o1}x + K_{o2}y)] \left\{ (\underline{K}_{o3} + K_{o3}) \exp[i\underline{K}_{o3}\xi] + (\underline{K}_{o3} - K_{o3}) \exp[-i\underline{K}_{o3}\xi] \right\}$$

$$\text{for } \xi < 0 \tag{2}$$

$$\psi_m = \frac{1}{K_v L^{3/2}} \exp[i(K_{o1}x + K_{o2}y)] \, 2\underline{K}_{o3} \exp[i\underline{K}_{o3}\xi] \qquad \text{for } \xi > 0,$$

where

$$V_o = \frac{\hbar^2}{2m} K_o$$

$$K_o{}^2 = K_{o1}{}^2 + K_{o2}{}^2 + K_{o3}{}^2$$

$$\underline{K}_{o3}{}^2 = K_{o3}{}^2 + K_{v_o}{}^2$$

$$\underline{K}_o{}^2 = K_o{}^2 + K_{v_o}{}^2.$$

Here, subscripts $1, 2, 3$ correspond to x, y, z directions, bars under K's indicate that the energy is measured from the bottom of the conduction band, and K_o and K_{o3} are both positive imaginary numbers.

For the atom, a hydrogen 2s wave function is fitted to the accurate Hartree-Fock 6s cesium wave function[8] to yield

$$\psi_a = \frac{a_1^{3/2}}{\sqrt{\pi}} (1-ar) e^{-ar}, \tag{3}$$

with $a = 0.755 \text{ Å}^{-1}$, and $a_1 = 0.6 \text{ Å}^{-1}$.

The perturbation is taken to be the potential of the ion core as seen by a metal electron. While this is the perturbation for the backward transition, not the transition from atom to metal, it is valid to use it for the perturbation of the atom-to-metal transition as has been pointed out by others.[9,10] Thus the perturbation is

$$H' = \frac{q^2}{r}. \tag{4}$$

Combining Eqs. 1 and 4, using the usual density of states function, and performing the necessary mathematical operations[4] the final result for the transition probability

$$w = \frac{4a_1^3 aq^2 \underline{K} s^3 e^{-2as}}{K_v^2 a_o \hbar} \left\{ 1 - \frac{4}{a^2 s^2} + \frac{8}{a^4 s^4} \right\}, \tag{5}$$

where $a_o = \hbar^2/mq^2$, and $\underline{K}$ is the wave number equivalent of the energy (measured from the bottom of the conduction band) of the electron involved in the transition. As can be seen, when the atom-metal separation goes to infinity (corresponding to no interaction), the transition probability goes to zero.

The effective lifetime τ of an atom before becoming an ion is given by the reciprocal of w, or

$$\tau = \frac{1}{w}. \tag{6}$$

This finite lifetime of the quantum state gives rise to a natural broadening of the atomic level, because of the uncertainty principle. The bandwidth is given by

$$\Gamma(s) \geqslant \hbar w(s) = \frac{\hbar}{\tau}.$$

4. Numerical Results

Using the reported values[11,12] of $\mu = 6.5$ ev, $E = 1.05$ ev, and $\phi_e = 4.6$ ev, for cesium on tungsten, Eq. 6 is evaluated as a function of atom distance from the surface. The lifetime τ and the bandwidth Γ are plotted as a function of s, in a hybrid but unambiguous manner in Fig. XII-25.
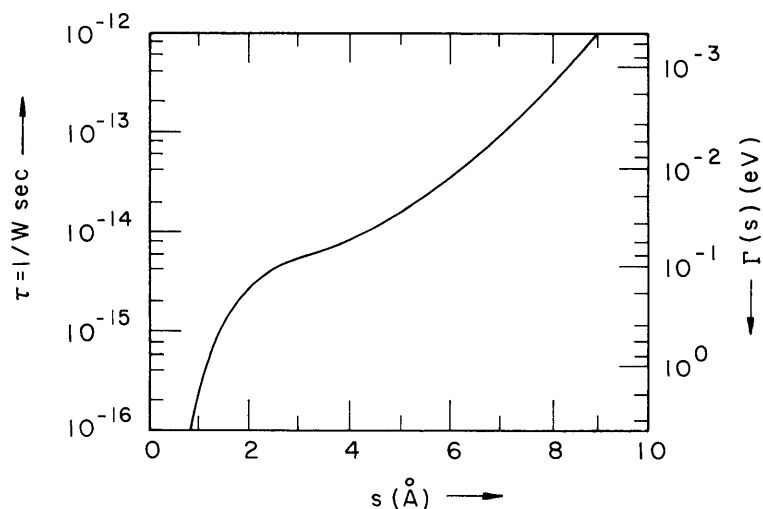

Fig. XII-25. Atomic lifetime and bandwidth as a function of distance from the surface.

If the distance of an adsorbed particle from the surface is taken to be 2.65 Å, the usual value of the so-called atomic radius, then the lifetime of the atomic state on the surface is found to be $\sim 5 \times 10^{-15}$ second. The bandwidth is ~ 0.15 ev, a value lying between that required for validity of either Rasor's or Gomer's theory.

5. Discussion and Conclusions

Note that the mechanism for bonding of cesium upon a metal surface proposed by Rasor and by Gomer are inconsistent with the results of this analysis. Some of the fea-

tures of the Levine model, however, are in complete accord with the results presented here, and in fact require these results. This will now be explained.

If an atom is brought to a surface at zero temperature, three distinct types of bonds can be formed. A completely ionic bond occurs if there is no overlap of conduction band
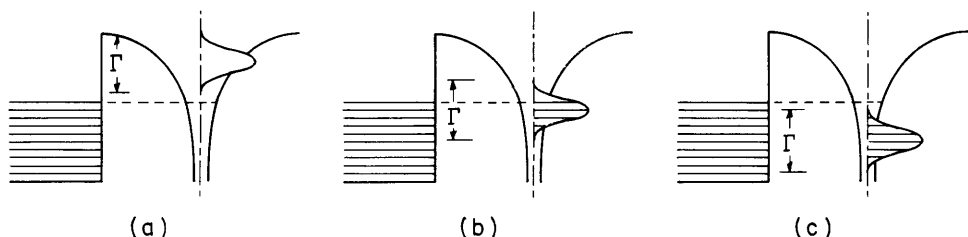

Fig. XII-26. (a) Ionic bonding. (b) Partially ionic-partially covalent bonding.
(c) Polar metallic or covalent type of bonding.

and broadened atomic level as shown in Fig. XII-26a. This is the required situation for validity of Rasor's model. If the atom and metal have some overlap as shown in Fig. XII-26b, a partially ionic-partially covalent bond will form. Levine requires this situation, although it is not stated explicitly in his analysis. A word of caution on Levine's theory, though. He feels a partially ionic-partially covalent bond forms between adsorbate atoms and four substrate atoms. This is not really true, for a partially ionic-partially covalent bond is actually formed between the atomic electrons and the free conduction electron of the metal, not electrons associated with a particular substrate atom. Identifying a metal electron with a particular ion core is a meaningless concept. Figure XII-26c shows the conditions required for the adsorption mechanism proposed by Gomer.

As the temperature is raised above zero, some conduction electrons are found at levels overlapping the broadened level of the adsorbate as shown in Fig. XII-27, where
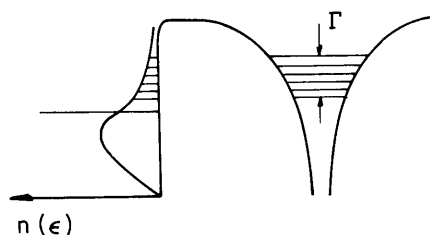

Fig. XII-27. Conduction-band electrons available for
covalent bonding at T > 0°.

the distribution function is superposed on the metal-atom drawing. In this situation, the conditions being those that occur experimentally, the bond formed between adsorbate and metal would be partially ionic-partially covalent if the broadening of the atomic level is

by the amount calculated in this analysis. Thus it is understandable why the Levine model, despite the incorrect picture of a CsW_4 molecule, gives good results. It proposes the correct form of bond. The only reason that the ionic bond model gives good results is that it includes so many adjustable constants hidden under the label of physical constants.

A final check on the validity of the ionic-covalent bond will be made in the future. Levine has proposed that the energy of adsorption for the ionic-covalent bond is the geometric mean of the energy of adsorption for purely ionic and purely covalent bonding. The purely ionic bond energy of adsorption can be calculated from Rasor's model. We intend to compute the actual covalent bond energy by calculating the exchange energy for two electrons, one electron being in the metal at an energy within the energies of the broadened band, and the other within the atom. This is the theoretical purely covalent bond energy for an adsorbate and a metal. Following Levine's claim, based on the Pauling type of argument, we should obtain the theoretical atomic energy of adsorption. This should agree with experimentally determined values, and thus serve to prove that the bond formed between a cesium atom and a metal surface is partially ionic-partially covalent.

J. W. Gadzuk

References

1. E. P. Gyftopoulos and J. D. Levine, J. Appl. Phys. 33, 67 (1962).

2. R. Gomer and L. W. Swanson, J. Chem. Phys. 38, 1613 (1963).

3. N. S. Rasor and C. Warner, J. Appl. Phys. 35, 2589 (1964).

4. J. W. Gadzuk, Adsorption Physics of Alkali Metal Vapors on Metal Surfaces — Cesium-Tungsten, S. M. Thesis, Department of Mechanical Engineering, M. I. T., January 1965.

5. H. D. Hagstrum, Phys. Rev. 96, 336 (1954).

6. D. Sternberg, Ph. D. Thesis, Department of Physics, Columbia University, New York, 1957.

7. H. D. Hagstrum, Phys. Rev. 122, 83 (1961).

8. A. Russek, C. H. Sherman, and D. E. Flinchbough, Phys. Rev. 126, 573 (1962).

9. D. R. Bates, A. Fundaminsky, and M. S. W. Massey, Trans. Roy. Soc. (London) 243, 93 (1950).

10. D. R. Bates (ed.), Atomic and Molecular Processes (Academic Press, New York and London, 1962), p. 572.

11. M. F. Manning and M. I. Chodorow, Phys. Rev. 56, 787 (1939).

12. J. B. Taylor and I. Langmuir, Phys. Rev. 44, 423 (1933).